

Alma Mater Studiorum Università di Bologna
Archivio istituzionale della ricerca

Tectonic setting and geochronology of the Cadomian (Ediacaran-Cambrian) magmatism in Central Iran, Kuh-e-Sarhangi region (NW Lut Block)

This is the final peer-reviewed author's accepted manuscript (postprint) of the following publication:

Published Version:

Rossetti, F., Nozaem, R., Lucci, F., Vignaroli, G., Gerdes, A., Nasrabadi, M., et al. (2015). Tectonic setting and geochronology of the Cadomian (Ediacaran-Cambrian) magmatism in Central Iran, Kuh-e-Sarhangi region (NW Lut Block). JOURNAL OF ASIAN EARTH SCIENCES, 102, 24-44 [10.1016/j.jseaes.2014.07.034].

Availability:

This version is available at: <https://hdl.handle.net/11585/653073> since: 2021-12-03

Published:

DOI: <http://doi.org/10.1016/j.jseaes.2014.07.034>

Terms of use:

Some rights reserved. The terms and conditions for the reuse of this version of the manuscript are specified in the publishing policy. For all terms of use and more information see the publisher's website.

This item was downloaded from IRIS Università di Bologna (<https://cris.unibo.it/>).
When citing, please refer to the published version.

(Article begins on next page)

This is the final peer-reviewed accepted manuscript of

Rossetti, Federico; Nozaem, Reza; Lucci, Federico; Vignaroli, Gianluca; Gerdes, Axel; Nasrabadi, Mohsen; Theye, Thomas: Tectonic setting and geochronology of the Cadomian (Ediacaran-Cambrian) magmatism in Central Iran, Kuh-e-Sarhangi region (NW Lut Block). JOURNAL OF ASIAN EARTH SCIENCES 102. 1367-9120

DOI: 10.1016/j.jseaes.2014.07.034

The final published version is available online at:

<http://dx.doi.org/10.1016/j.jseaes.2014.07.034>

Rights / License:

The terms and conditions for the reuse of this version of the manuscript are specified in the publishing policy. For all terms of use and more information see the publisher's website.

This item was downloaded from IRIS Università di Bologna (<https://cris.unibo.it/>)

When citing, please refer to the published version.

Tectonic setting and geochronology of the Cadomian (Ediacaran-Cambrian) magmatism in Central Iran, Kuh-e-Sarhangi region (NW Lut Block)

Federico Rossetti ^{a,*}, Reza Nozaem ^b, Federico Lucci ^a, Gianluca Vignaroli ^a, Axel Gerdes ^c, Mohsen Nasrabadi ^b, Thomas Theye ^d

^a *Dipartimento di Scienze, Università degli Studi Roma Tre, Roma, Italy*

^b *Department of Geology, Imam Khomeini International University, Qazvin, Iran*

^c *Institut für Geowissenschaften, Goethe Universität, Frankfurt, Germany*

^d *Institut für Mineralogie, Universität Stuttgart, Stuttgart, Germany*

ARTICLE INFO

Keywords:

Arc magmatism
Transpressional orogens
Cadomian
Gondwana assembly Lut
Block
Iran

ABSTRACT

The structure, age and petrogenesis of plutonic basement rocks from the Kuh e Sarhangi region, located in the Kashmar Kerman tectonic zone of Central Iran are described. These intrusive rocks consist of a sub alkaline, dominantly high K calc alkaline acidic suite, characterised by high SiO₂ (72.60–77.17 wt%), and alkalis (up to 8 wt%) and low Mg# (0.7–3.5). They are also enriched in Th, U and light rare earth elements, and depleted in Nb, Ta, and Ti, thus showing a geochemical fingerprint compatible with arc magmatism. The U–Pb zircon geochronology constrains magma crystallisation and emplacement during Ediacaran–Cambrian (ca. 575–535 Ma) times, under a tectonic regime dominated by transpressional tectonics as constrained by analysis of field structures. Combined inverse and forward modelling thermobarometry indicates pluton emplacement occurred in a thickened crustal environment, suggesting the Kuh e Sarhangi magmatic belt exposes the exhumed roots of a volcanic arc. This magmatism is interpreted as part of the Cadomian, subduction related magmatism and framed within an oblique convergence scenario during formation of an Andean type active margin all along the northern (proto Tethyan) margin of the Gondwana Supercontinent.

1. Introduction

The Neoproterozoic–Cambrian time frame was dominated by the growth of the Gondwana Supercontinent that resulted from a long lived history of orogenic construction, starting from the breakup of Rodinia (870–800 Ma) to the final amalgamation in Cambrian times (e.g. Dalziel, 1991; Meert, 2003; Boger and Miller, 2004; Collins and Pisarevsky, 2005; Cawood, 2005; Cawood and Buchan, 2007; Li et al., 2008; Torsvik and Cocks, 2013; Nance et al., 2014). The terminal assembly of Gondwana largely occurred between around 570 and 500 Ma and was achieved through accretion of various continental blocks both involving prolonged collisional assembly of East and West Gondwana continents (Kuunga–Malagashi orogeny; Meert, 2003; Collins and Pisarevsky,

2005; Meert and Lieberman, 2008) and development of subduction systems all along the margins of the Gondwana supercontinent (Terra Australis Orogen and North India Orogen; Boger and Miller, 2004; Cawood, 2005; Cawood et al., 2007; Murphy et al., 2011).

Occurrence of voluminous Cadomian (Ediacaran–Cambrian) subduction related magmatism in basement terranes from Himalaya, to Iran, Turkey and Greece attests for formation of an Andean type active margin all along the northern (proto Tethyan) margin of the Gondwana Supercontinent (Ramezani and Tucker, 2003; Gessner et al., 2004; Cawood et al., 2007; Hassanzadeh et al., 2008; Horton et al., 2008; Ustaömer et al., 2009; Saki, 2010; Azizi et al., 2011; Mahmoud et al., 2011; Zhu et al., 2012; Hu et al., 2013; Jamshidi Badr et al., 2013; Shafaii Moghadam et al., in press). Within this general framework, the late Neoproterozoic–Cambrian basement rocks of Iran are generally interpreted as of the dispersed fragments of this Cadomian active margin that extended from NW Africa to India (cfr. Ramezani and Tucker, 2003; Ustaömer et al., 2009; Shafaii Moghadam et al., in press) (Fig. 1).

* Corresponding author. Address: Dipartimento di Scienze, Sezione Scienze Geologiche, Università degli Studi Roma Tre, Largo S. L. Murialdo, 1, 00146 Roma, Italy. Tel.: +39 0657338043; fax: +39 0657338201.

E-mail address: federico.rossetti@uniroma3.it (F. Rossetti).

However, some paleotectonic reconstructions for the Gondwana Supercontinent during early Cambrian frame Central Iran into a passive margin setting (e.g., Torsvik and Cocks, 2009, 2013; Berra and Angiolini, 2014). In addition, still missing is the linkage between magmatism and the tectono metamorphic evolution of the country rocks, hampering a full understanding of the tectonic scenario during formation of the Cadomian arc in Iran.

In this paper we present field, structural, petrological and U Pb zircon laser inductively coupled plasma mass spectrometry (LA ICP MS) geochronological data with the aim to define the intrusive setting of a suite of granitoids emplaced within the metamorphic basement of the Kuh e Sarhangi region, NW Central Iran (Figs. 1b and 2). These data, integrated with structural and metamorphic investigations from the country rocks, are used to refine the

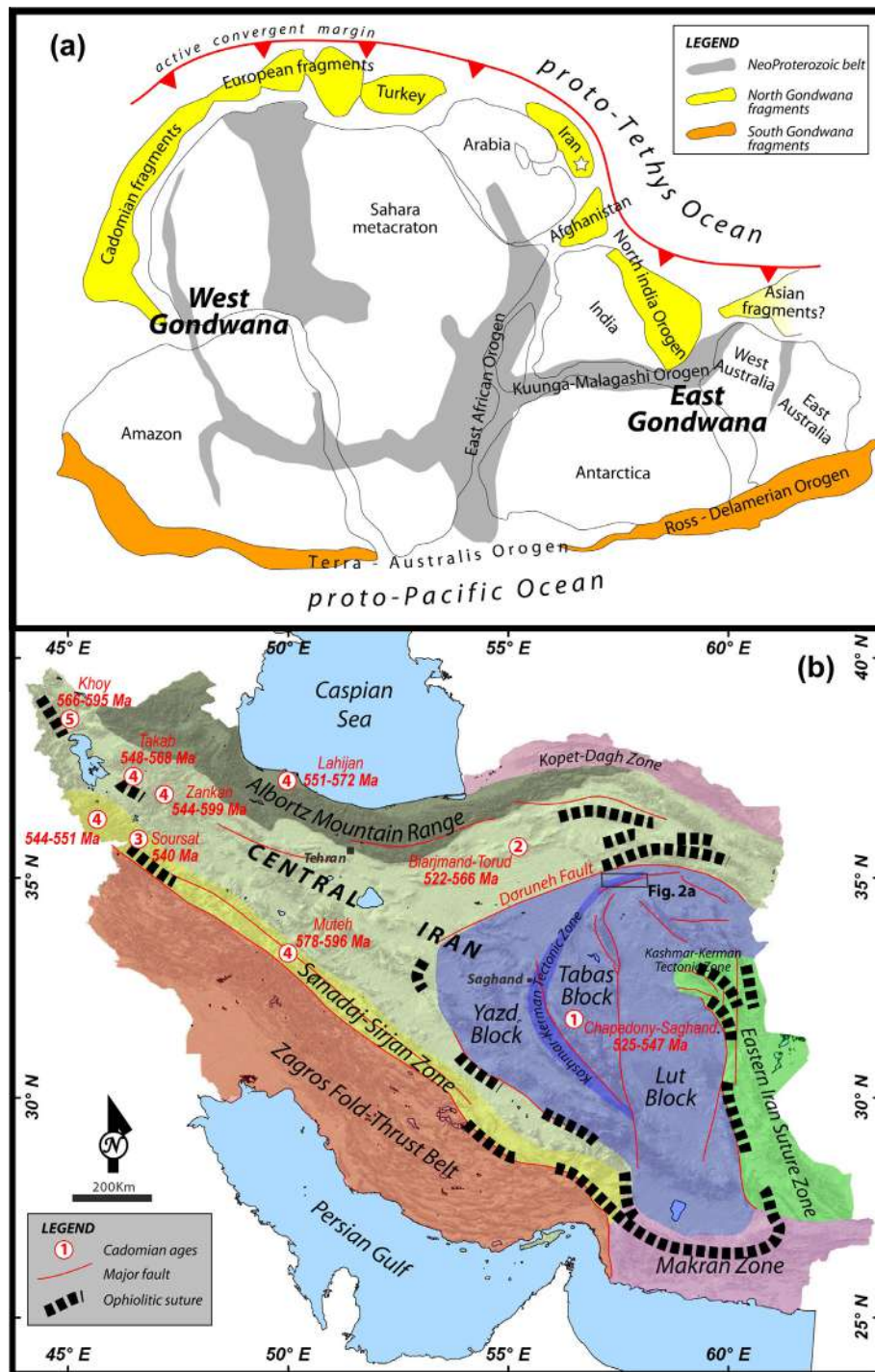


Fig. 1. (a) The configuration of the Gondwana Supercontinent at 550 Ma; the Cadomian terranes at the northern (proto-Tethyan) margin of the Gondwana Supercontinent are also indicated (modified and re-adapted after Cawood et al., 2007; Shafaii Moghadam et al., in press). The Cimmerian terranes of the Iran plate are indicated by a white star. (b) Schematic map showing the main lithotectonic domains in Iran (modified after Ramezani and Tucker, 2003). The map also shows distribution of the available Cadomian U–Pb zircon ages (numbered circles) and location of the study area. (1) Ramezani and Tucker (2003); (2) Shafaii Moghadam et al. (in press); (3) Jamshidi Badr et al. (2013); (4) Hassanzadeh et al. (2008); (5) Azizi et al. (2011).

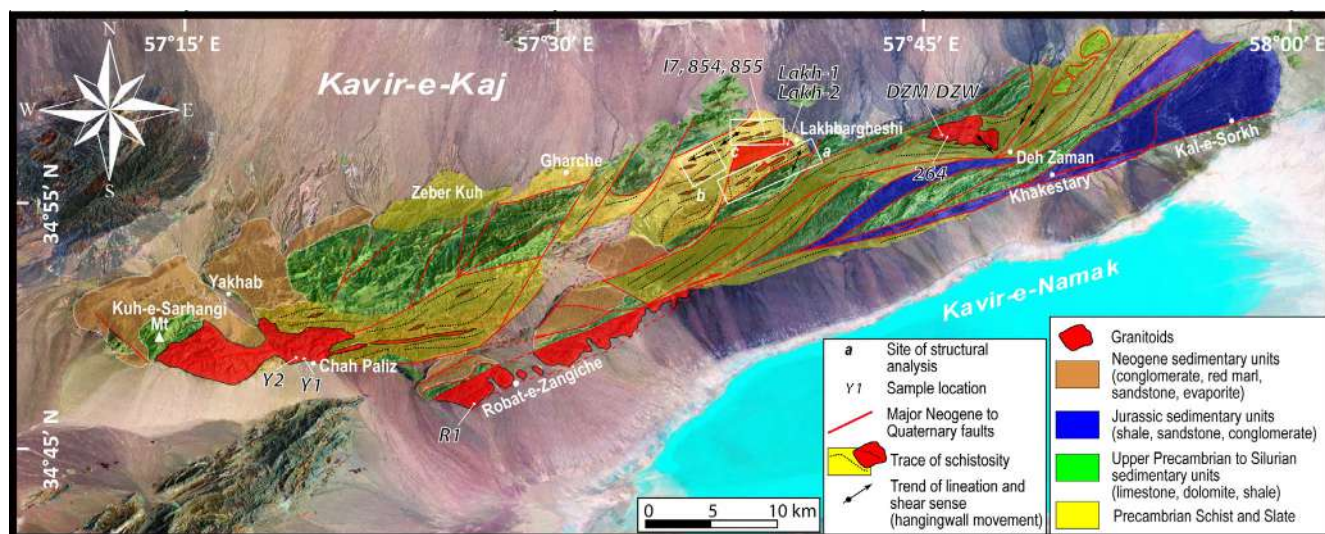


Fig. 2. Schematic geological-structural map of the Kuh-e-Sarhangi region (modified and re-adapted after Sahandi et al., 2011; Nozaem et al., 2013). Rectangles show location of areas of detailed structural field work and selected rock samples analysed in this study.

current understanding of the tectonic evolution during formation of the active Cadomian margin at the northern boundary of the Gondwana Supercontinent.

2. Geological background

The Central Iran Micro Continent (CIMC) is made of three major, fault bounded tectonic blocks, from west to east: the Yazd, Tabas, and Lut, respectively (Takin, 1972) (Fig. 1b). These are continental fragments (also called Cimmerian terranes) that drifted away during the breakup of Gondwana and were accreted to Eurasia in Triassic times (e.g., Stöcklin, 1968; Berberian and King, 1981; Sengör, 1984; Alavi, 1991; Ramezani and Tucker, 2003; Bagheri and Stampfli, 2008). These tectonic blocks are bounded by major strike slip fault zones and have peculiar stratigraphy, deformation style and pattern of recent seismicity (Berberian, 1981).

The Gondwanan basement of Central Iran is considered to be Precambrian, and it is dominated by granitic to tonalitic gneiss of Ediacaran Cambrian ages (Ramezani and Tucker, 2003; Hassanzadeh et al., 2008; Shafaii Moghadam et al., in press; see Fig. 1b for distribution of the Cadomian ages in Iran). Recently, Nutman et al. (2014) reported zircon U Pb Hf isotopic data indicating derivation of the magmatic protoliths from heterogeneous Eoarchean Neoproterozoic (0.9–3.6 Ga) crustal components. The crystalline basement is overlain by Paleozoic sediments and a discontinuous Mesozoic and Cenozoic cover (Stöcklin, 1968).

The study area is located at the north western edge of the Lut Block and it is comprised within the Kashmar Kerman Tectonic Zone (Ramezani and Tucker, 2003), a nearly 600 km long, arcuate and structurally complex fault bounded belt that separates the Tabas and Yazd blocks (Figs. 1b and 2). This tectonic zone provides remarkable exposures of the deeper sections of the central Iran basement rock series, previously described as part of Zeber Kuh Range (Sahandi et al., 1983) and tentatively assumed as correlatives of the Proterozoic Cambrian Boneh Shurow Complex of the Saghand region, for which Cadomian U Pb zircon magmatic ages are reported (from ~547 to 525 Ma; Ramezani and Tucker, 2003) (Fig. 1b). Tertiary high grade metamorphic rocks and post kinematic intrusives also occur in the western part of the Saghand area (Chapedony Complex; Ramezani and Tucker, 2003), which have been interpreted as a major episode of Eocene Cordilleran style metamorphic core complex formation in Central Iran (Verdel et al., 2007; Karagaranbafghi et al., 2012).

Proterozoic and Cambrian basement units are reported in the central part of the study area, and record a prolonged history of deformation and polyphase reactivation (Sahandi et al., 2011; Nozaem et al., 2013). In particular, following Sahandi et al. (1983, 2011) these rock units comprise, from bottom to top: (i) medium to high grade metamorphic rocks (mostly garnet chlorite-amphibolite schists) that are exposed around Lakhbarghesi and southeast of Zeber Kuh (Fig. 2); (ii) the Rizu Formation (phyllites, metavolcanics, quartzites and dolomites); and (iii) the Late Ediacaran Lower Cambrian platform deposits (alternating shale and dolostone members) of the Soltanieh Formation (Stocklin et al., 1964; Jafari et al., 2007). A number of granitoid plutons also crops out in the study area (from NE to SW, hereafter referred as the Deh Zaman, Lakhbarghesi, Robat and Yakhab plutons, respectively; Fig. 2) that have been described to intrude sequences of different metamorphic grade as part of the Precambrian basement of Central Iran (Sahandi et al., 1983). No direct constraint on the age of these magmatic bodies or on the $P-T-t$ deformation history of the host rocks is available from the study area.

The cover rocks consist of (Sahandi et al., 2011): (i) Palaeozoic (Silurian Permian) weakly metamorphosed sequences of shales, limestones, sandstones and dolomites; (ii) Mesozoic sedimentary rocks including the Jurassic Garedu Red Beds and Cretaceous marls and limestones; and (iii) Neogene deposits, belonging to the Upper Red Formation (Rutner et al., 1970; Eftekharneshad et al., 1977) and made of alternating conglomerates, marls, sandstones and evaporites, which are unconformably covered by sub horizontal Quaternary alluvial deposits. The structural architecture of the study area is dominated by brittle Neogene Quaternary, NE-SW striking right lateral strike slip tectonics during development of the Kuh e Sarhangi Fault zone (Nozaem et al., 2013) (Fig. 2).

3. Field data and structures in the basement units

The overall structural architecture of the basement units in the Kuh e Sarhangi area, is characterised by steeply dipping foliation attitudes that are arranged to form a major, NE-SW striking steeply dipping shear belt (average thickness of ca. 20 km), where the basement rocks (including the granitoids) are involved. Remarkably, most of the granitoid bodies are texturally overprinted to form extensive gneissic bodies that occur as large scale (km size) shear lenses within a prominent ENE-WSW striking, steeply dipping mylonitic shear fabric. This ductile shear fabric is

subparallel to the trace of the Neogene Quaternary Kuh-e Sarhangi Fault zone (Nozaem et al., 2013) (Fig. 2).

Intrusive relationships, structures in granitoids, together with the main textural and metamorphic features in the metamorphic host rocks are described in the following sections. The host rocks grade from low grade phyllites and medium grade staurolite bearing micaschists (Deh Zaman) to garnet micaschists (Robat) and amphibolites (Lakhbargheshi). In particular, our field investigations are concentrated on Deh Zaman and Lakhbargheshi areas, where continuous sections from the country rocks to the granitoid intrusives are exposed and studied in detail. This information is integrated with petrographic/geochemical and age data as derived from sampling of the granitoid intrusions and country rocks exposed in the Yakhab and Robat areas (Fig. 2). Table 1 shows sample locations, together with their constituent mineralogy. Analytical methods are described in the Appendix A. Mineralogical abbreviations follow Whitney and Evans (2010).

3.1. Deh Zaman area

The Deh Zaman intrusive complex consists of a felsic composite body (samples DZM, DZW and 264 in Table 1) with an areal extent of ca. 15 km² (Fig. 3A), showing a general gneissic texture. Host rocks consist of chlorite muscovite phyllites, locally entering the staurolite andalusite metamorphic zone (samples 15 in Table 1) when approaching contacts with the intrusive bodies. Intrusive contacts are obliterated during development of the regional shear fabrics that affect both the country rocks and the granitoid intrusion (Fig. 3B). The Soltanieh dolomites are stretched apart and boudinaged along the main shear contact localised along the boundary with the schists. The shear deformation is associated with syn kinematic quartz vein arrays segregation that are observed to occur both in the intrusive bodies and the country rocks (Fig. 3C and D). The metapelite country rocks show a steeply dipping shear foliation, striking ENE–WSW (mean attitude: N232°, 70°) and bearing sub horizontal stretching lineations (mean pitch: 150°), provided by quartz muscovite aggregates. Shear foliation is deformed by subvertical trains of isoclinal folds, having steeply dipping NE–SW axial surfaces (proximal to the vertical; Fig. 3E). In the country rocks, the veins are folded, boudinaged and stretched along the shear foliation, but late stage sub vertical vein sets are locally observed to cut across the ductile shear fabrics. The sense of shear as derived from the S–C fabrics, arrangement of the vein arrays and tension gashes is systematically sinistral reverse, within a general scenario of progressive ductile to brittle shearing (Fig. 3F). The Deh Zaman intrusives show a granular texture and a prominent solid state mylonitic fabric. Shear foliation is subvertical and

striking from E–W (in the west portion of the granite body, being sub parallel to that in the country rocks) to NNW–SSE (in the eastern portion). Stretching lineations, as dominantly provided by quartz muscovite assemblages, indicate oblique slip (average pitch values of 135°) (Fig. 3E and G). The igneous assemblage consists of dominant alkali feldspar, plagioclase, quartz, biotite ± garnet with secondary biotite muscovite. At the thin section scale, feldspar grains occur as highly strained, fractured porphyroclasts embedded within a ductile deformed quartz phyllosilicate (biotite and muscovite) shear matrix. Sense of shear as deduced from sigma type garnet and feldspar porphyroclasts, oblique foliation and S–C shear fabrics is sinistral reverse (Fig. 4A and B).

3.2. Lakhbargheshi area

The Lakhbargheshi pluton (samples Lakh 1–2 in Table 1) covers an exposure of about 20 km². The magmatic body displays a lensoid shape, elongated along a mean NE–SW direction (Fig. 2). Contacts with the country rocks are steeply dipping and gradational in the field (Fig. 5A). The Lakhbargheshi body displays a massive isotropic texture, only overprinted by late stage fracturing (Fig. 5B). At the thin section scale, magmatic fabric is well preserved, with polygonal, coarse grained quartz feldspar matrix, with scattered grains of biotite and euhedral epidote. Quartz microfabrics only show limited effects of ductile strain, mostly documented by patchy undulose extinction (Figs. 4C and D and 5B). The host rock consists of a sequence of alternating (from metre to cm scale) metapelites and metabasites (samples 854, 855, and 17 in Table 1), where a progressive transition from plano linear to well annealed static fabrics is observed when approaching contacts with the intrusive body (Fig. 5C and D). This textural change is also associated with a prograde metamorphic zonation in the field, as typified by the transition from epidote to garnet amphibolites in the metabasite country rocks. Plano linear fabric in the country rocks consists of a NE–SW striking steeply dipping foliation (mean strike: N255°) with dominant oblique stretching lineations (Fig. 6, stereoplots a and c), developed during intense non coaxial deformation, syn kinematic relative to the amphibolite grade metamorphism. Solid state S–L fabrics are also documented from felsic magmatic bodies intruded into the country rock, which occurs as metre sized intrafoliar orthogneiss boudins and shear lenses, concordant with the regional foliation. These granitoid bodies show a solid state, subvertical, NE–SW striking shear foliation that bear a prominent oblique stretching lineation, as provided by quartz muscovite aggregates (Figs. 5E and 6b). Sense of shear, both documented at the meso and micro scale, is systematically sinistral reverse (Figs. 5F). At the thin section scale, shear foliation in the gneissic lenses is defined by muscovite flakes

Table 1

List of the analysed samples, with geographical location, constituent mineralogy and analytical methods adopted.

Label	Rock type	Position		Mineralogical assemblage	Analytical methods		
		Latitude (°N)	Longitude (°E)		ICPMS	U–Pb (Zrn)	EMPA
DZM	Granitoid	34.962944°	57.770184°	Qz, Pl, Kfs, Grt, Bt, Ms, ± Zrn, Ap, Mag, Chl Qz,	Yes	Yes	Yes
DZW	Granitoid	34.960732°	57.780701°	Pl, Kfs, Grt, Bt, Ms, ± Zrn, Ap, Mag, Chl Qz, Pl,	Yes	Yes	Yes
264	Granitoid	34.960732°	57.780701°	Kfs, Grt, Bt, Ms, ± Zrn, Ap, Mag, Chl Qz, Pl, Kfs,	Yes		Yes
Lakh-1	Granitoid	34.953555°	57.658914°	Bt, Ep, ± Grt, Zrn, Ap, Ttn	Yes	Yes	Yes
Lakh-2	Granitoid	34.951671°	57.655315°	Qz, Pl, Kfs, Bt, Ep, ± Grt, Zrn, Ap, Ttn	Yes		Yes
17	Grt Amphibolite	34.951345°	57.655708°	Amp, Qz, Pl, Grt, Ep, Ilm ± Bt			Yes
855	Grt Amphibolite	34.951345°	57.655708°	Amp, Qz, Pl, Grt, Ep, Ilm ± Bt			Yes
854	Micaschist	34.951345°	57.655708°	Pl, Qz, Grt, Ilm, Ms, Amp ± Pa			Yes
R1	Granitoid	34.783274°	57.446614°	Qz, Pl, Kfs, Bt + Grt, Bt, Ms, ± Zrn, Ap, Mag, Chl	Yes	Yes	Yes
Y1	Granitoid	34.815423°	57.301869°	Qz, Pl, Ms, Ep ± Kfs, Zrn, Ttn, Ap, Mag	Yes	Yes	Yes
Y2	Granitoid	34.816104°	57.298883°	Amp, Pl, Qz, Ms, Ep, Rt, Zrn, Ap, Mg	Yes		Yes

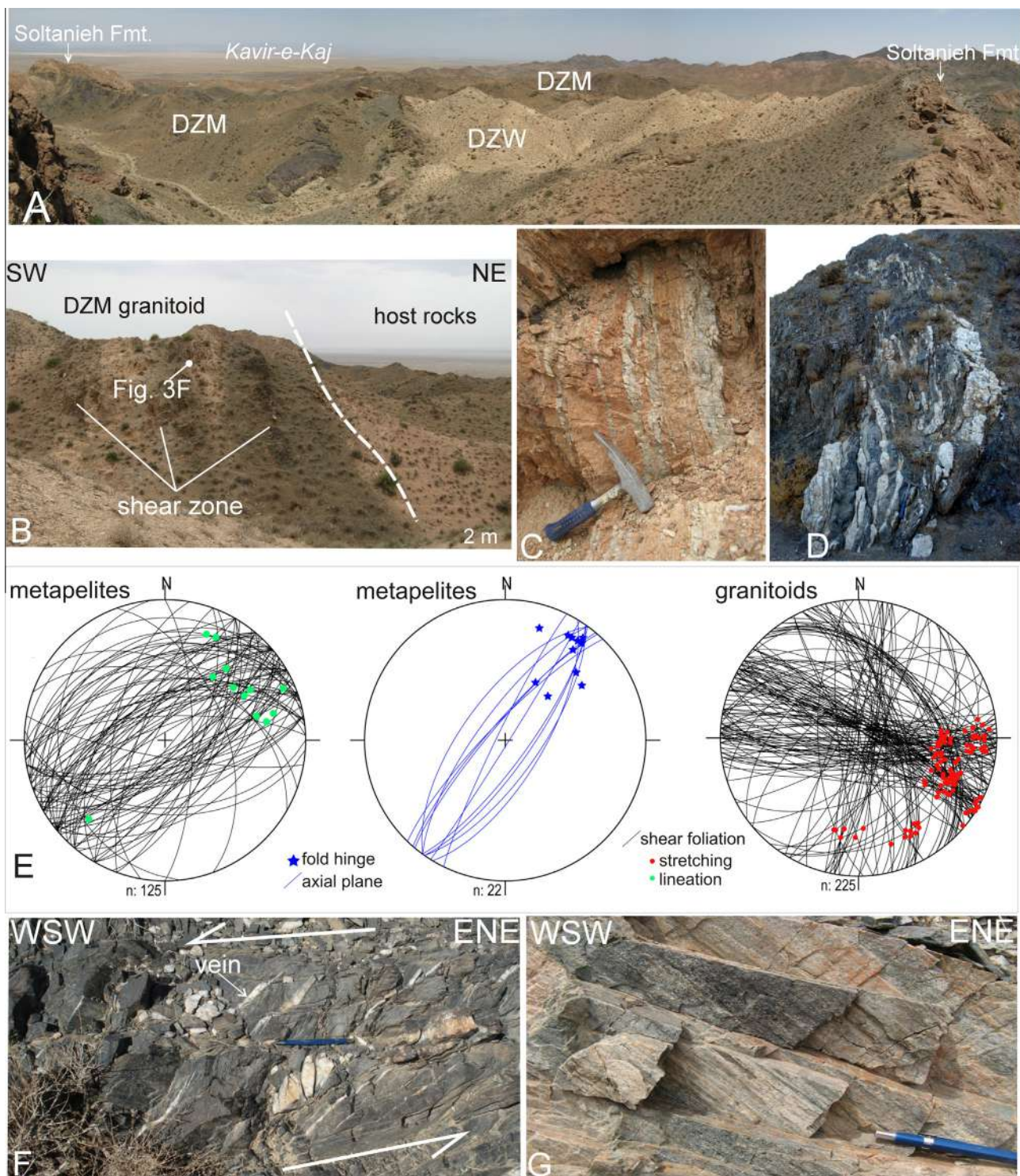


Fig. 3. (A) Exposure of the Deh Zaman intrusive complex, showing contacts with country rocks and the field relationships between the leucocratic (DZW) and the melanocratic (DZM) magmatic bodies. (B) Steeply-dipping tectonic contact between the Deh Zaman intrusive body (DMZ) and the Pre-Cambrian metapelite country rocks. The granitoid is affected by distributed, subvertical mylonitic shear zones. (C) A subvertical array of quartz veins that cut across the DZM body. (D) Steeply-dipping, folded and boudinaged quartz veins in the Pre-Cambrian metapelite country rocks (host rocks of the Deh Zaman intrusives). (E) Equal-area stereoplots (Schmidt net, lower hemisphere projection) showing shear zone plano-linear fabrics and fold attitudes in the Deh Zaman area. (F) En-echelon array of quartz veins indicating sinistral shearing in Pre-Cambrian metapelites (view from above). (G) Oblique (quartz-muscovite) stretching lineations in the steeply dipping gneissic foliation of the DZM granite.

and quartz ribbons flowing around porphyroclastic feldspar grains. Quartz grains show evidence of dynamic recrystallisation, typically documented by core and mantle microstructures, with relics of large, strained grains showing diffuse undolose extinction, deformation bands and subgrain formation, mantled by strain free

smaller size recrystallised grains. Feldspar grains show minor evidence of ductile creep, seldom attested by patchy undolose extinction in some grains and by plagioclase re crystallisation. Feldspar grains are also largely affected by brittle (micro) cracking. Micro-scale shear sense indicators are provided by oblique foliation,

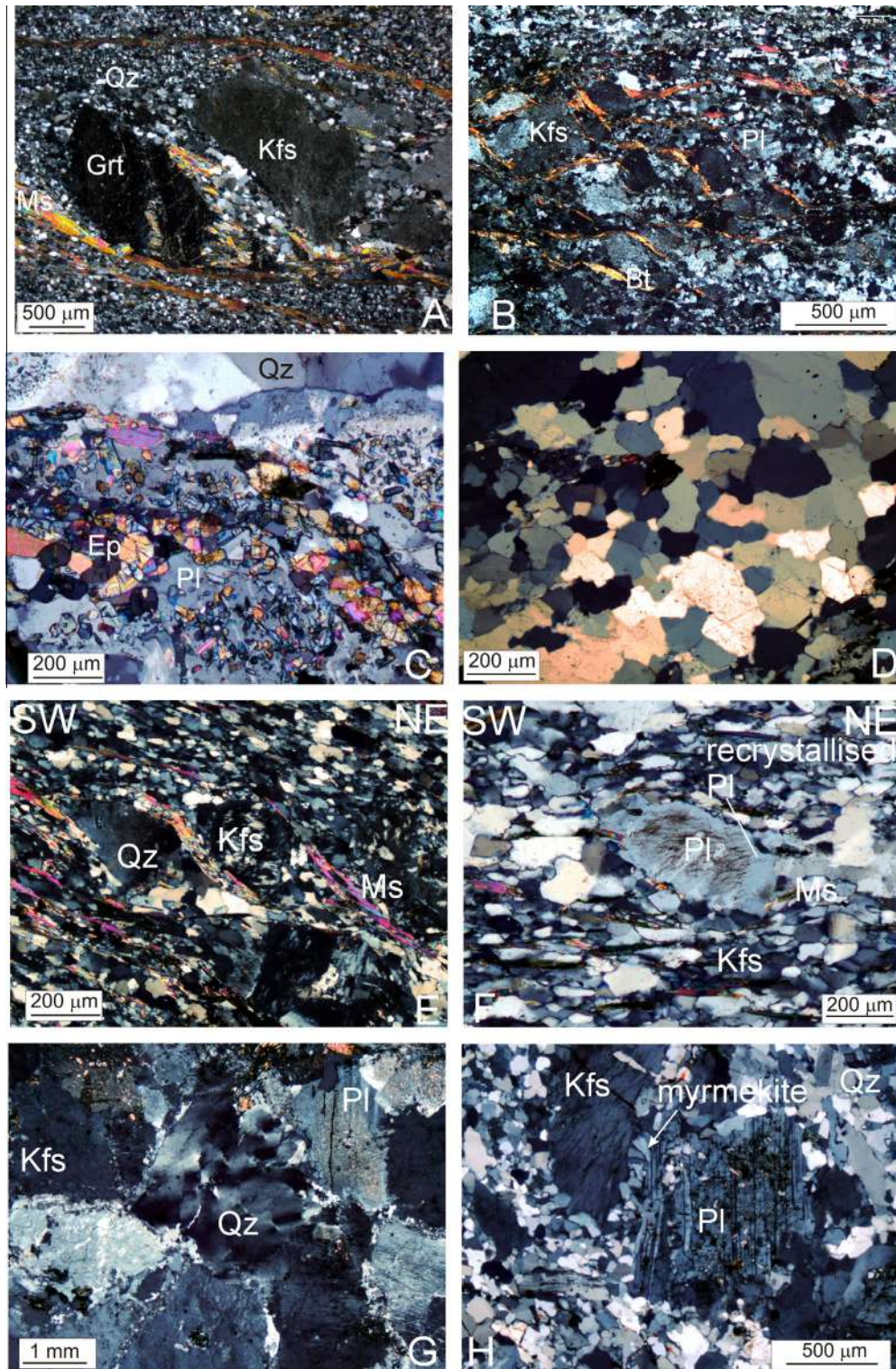


Fig. 4. Granite microtexture. (A) Mylonite fabric in the Deh Zaman granitoids (DZM sample), showing sigma-shaped garnet (Grt) and K-feldspar (Kfs) porphyroclasts, mica (Ms) fishes and oblique foliation made of recrystallised quartz (Qz). Sense of shear is sinistral (crossed polars; thin section cut parallel to the stretching lineations and normal to mylonitic foliation). (B) S-C fabric defined by feldspar porphyroclasts embedded in fine grained recrystallised quartz matrix and biotite folia (DZM sample). Sense of shear is sinistral (crossed polars; thin section cut parallel to the stretching lineations and normal to mylonitic foliation). (C) Detail of the primary igneous assemblage made of Epidote (Ep), quartz (Qz), plagioclase (Pl) in the Lakhbargheshi pluton (sample Lakh-1). Quartz grains show only minor evidence of strain as indicated by patchy undulose extinction (crossed polars). (D) Well annealed, strain free quartz microfabric in the Lakhbargheshi pluton (sample Lakh-1; crossed polars). (E) S-C, mylonitic fabric in a sheared granitoid lense within the country rocks of the Lakhbargheshi pluton. Augen feldspar (Kfs)-quartz (Qz) aggregates occur into elongated lenses of fine recrystallised and ribbon quartz and syn-kinematic muscovite (Ms) foliation. Sense of shear is sinistral (crossed polars; thin section cut parallel to the stretching lineations and normal to mylonitic foliation). (F) Ductile deformed plagioclase (Pl) porphyroclast with recrystallised tails in a recrystallised matrix of quartz grains that define oblique foliation in a sheared granitoid body from the country rocks of the Lakhbargheshi pluton. Sense of shear is sinistral as also indicated by the muscovite mica fishes (crossed polars; thin section cut parallel to the stretching lineations and normal to mylonitic foliation). (G) Fractured and strained feldspar grains coexisting with strongly deformed quartz (Qz) grains with blocky sub-grains in the Yakhab pluton (sample Y1). Note also the fine recrystallised rims surrounding both K-feldspar (Kfs) and plagioclase (Pl) grains (crossed polars). (H) Myrmekite (symplectic intergrowth of quartz and sodic plagioclase) replacement of igneous K-feldspar (Kfs) along the K-feldspar-plagioclase (Pl) interface in the Robat granitoid (sample R1; crossed polars).

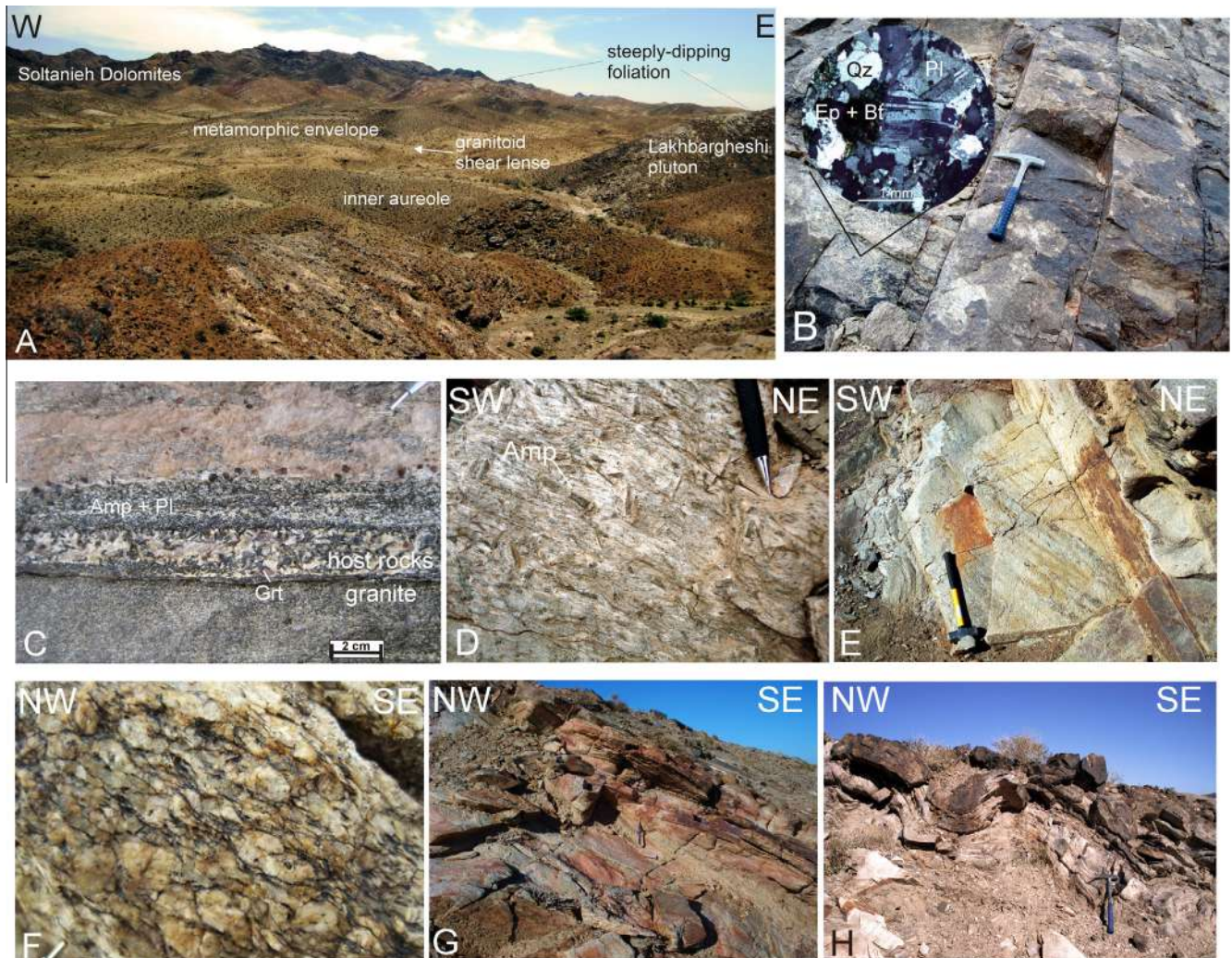


Fig. 5. Lakhbargheshi area. (A) Panoramic view showing the Pre-Cambrian country rocks surrounding the Lakhbargheshi pluton. Regional foliation is steeply-dipping, wrapping around the intrusive body. (B) The massive texture of the Lakhbargheshi pluton at meso-scale. The inset shows the magmatic texture and mineral assemblage (made of quartz (Qz), plagioclase (Pl), epidote (Ep), biotite (Bt) at the microscale (crossed polars; sample Lakh-1). (C) A portion of the granite-host rock contact, showing the immediate envelope of the Lakhbargheshi pluton made of garnet (Grt)-bearing metabasite–metapelite alternates. (D) Linear fabric in S–L tectonites from the host rocks of the Lakhbargheshi pluton as defined by Ca-amphibole (Amp) porphyroblasts in the main mylonitic foliation. (E) Oblique (quartz–muscovite) stretching lineations in sheared granitoids from the host rocks. (F) Meso-scale shear sense indicators in a mylonitised granitoid shear lense. Kinematics is provided by S–C fabric and sigma-type feldspar porphyroclasts (section normal to main shear foliation and parallel to the stretching lineations). (G) Recumbent isoclinal folding of a granitoid lense in the country rocks. The fold asymmetry indicates a NW vergence. (H) Late-stage, open upright folds reworking the S–L tectonites in the envelope of the Lakhbargheshi pluton.

S C fabrics, sigma type porphyroclasts and mica fishes (Fig. 4E and F). Shear foliation development is accompanied by folding, evolving from isoclinal to open, upright geometries. The fold axial surfaces strike NE SW (Fig. 6), and the fold vergence usually indicates a top to the NW tectonic sense of transport (Figs. 5G H).

3.3. Yakhab and Robat areas

The Yakhab granitoid (samples Y1 and Y2 in Table 1) crops out at the southwestern termination of the Kuh e Sarhangi Massif and covers an area of about 35 km². Contacts with the country rocks are poorly exposed; when observed, they are severely overprinted by brittle faulting associated with the Kuh e Sarhangi fault system (Nozaem et al., 2013). At the north of Chah Paliz village (Fig. 2), subvertical, NE SW striking apophyses of the Yakhab granitoids are observed to intrude the Precambrian metamorphics that dominantly consists of garnet biotite micaschists. The magmatic mineralogy consists of K feldspar, plagioclase, quartz, epidote, garnet ± biotite; seldom, plagioclase grains are altered to secondary epidote muscovite aggregates. At the meso scale, the Yakhab

granitoid appears as strongly fractured with distributed cataclastic horizons; evidence of ductile deformation is limited to some elongate quartz grains with weak development of solid state foliation. At the thin section scale, the crystal plastic deformation of quartz grains varies from weak undolose extinction to blocky subgrain formation. Heterogeneous is also the feldspar microfabrics, dominated by diffuse microcracking and undolose extinction in the highly strained domains (Fig. 4G).

The Robat granitoid (sample R1 in Table 1) covers an area of about 22 km² at the southern edge of the study area. Contacts with the country rocks (Paleozoic sequences) are controlled by major brittle fault systems developed along the main damage zone of the Kuh e Sarhangi Fault. Similarly to the Yakhab granitoid, the Robat pluton shows a cataclastic appearance at the meso scale. At the thin section scale ductile deformation in quartz is attested by undolose extinction and subgrain formation and dynamic recrystallisation. Feldspar grains usually have microfractures and undolose extinction. In the highly strained domains Myrmekite formation along the K feldspar/plagioclase boundaries are also locally observed (Fig. 4F).

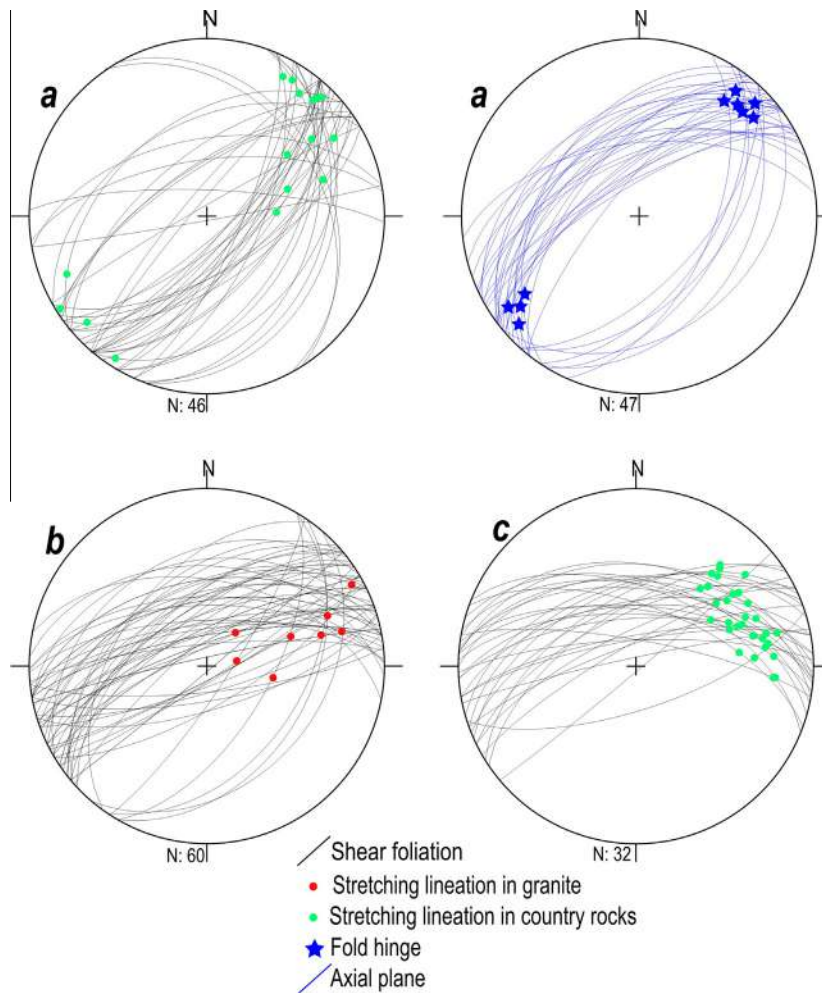


Fig. 6. Equal-area stereoplots (Schmidt net, lower area projection) showing attitude of the plano-linear fabrics in the Lakhbargheshi area (a, b, c indicate areas of structural investigations; see Fig. 2).

4. Petrography and geochemistry of the granitoid rocks

The studied granitoids consist of medium to coarse grained rocks, composed mainly of quartz (30–50 vol.%), alkali feldspar (30–40 vol.%) and sodic plagioclase (5–31 vol.%). Accessory phases (>10 vol.%) include garnet (Alm–Grs solid solution), epidote, biotite, Fe–Ti oxides, apatite, zircon, and allanite (Table 1; for analytical details see Appendix A). Granitoid microtextures vary from undeformed to mylonitic and are characterised by fine to coarse (0.1–1 mm in linear size) inequant grains that typically show interdigitating phase boundaries. In strained lithotypes, solid state deformation is typified by quartz ductility (undolose extinction and recrystallisation) and feldspar microcracking. Feldspar fracturing is usually accompanied by development of mortar texture together with mimetic growth of secondary muscovite. A late alteration stage is attested by the diffuse growth of chlorite after biotite, and by fine grained white mica/epidote aggregates after plagioclase.

Feldspars consist of both sodic plagioclase ($X_{An} = 6–31\%$) and alkali feldspar ($X_{Ab} = 89–99\%$ and $X_{Or} = 89–98\%$); both perthites ($X_{Ab} = 28\%–X_{Or} = 71\%$) and antiperthites ($X_{Ab} = 79\%–X_{Or} = 20\%$) exolutions occur in alkali feldspar. Variable BaO contents (up to 1.53 wt%) are measured. The garnet compositions broadly correspond to an Alm–Grs solid solution (Alm_{58–70}Grs_{19–31}Prp_{3–9}Sps_{0–13}) with moderate core to rim chemical zonation,

characterised by a rimward decrease in the Sps component compensated by Alm enrichment and flat Grs and Prp. In the Lakhbargheshi samples (Lackh 1–2 in Table 1), garnet is richer in Grs (Alm_{30–45}Grs_{35–45}Py_{0–1}Sps_{13–18}). Biotite, with a grain size from

~0.5 to 3 mm in length, is enriched in TiO₂ (up to 3.01 wt%) with X_{Mg} ($[MgO]/[MgO + FeO] = 0.31–0.38$). Primary epidote, which is observed in samples Lackh 1 and Y1, occurs mostly as euhedral grains (up to 1 mm in length) adjacent to biotite, in contacts with plagioclase and quartz. Secondary epidote is mostly found as alteration products of igneous plagioclase. Primary epidote has restricted pistacite (Ps, atomic $[Fe^{3+}]/[Fe^{3+} + Al^{3+}]$) content between 21% and 26%, whereas secondary one has lower Ps (17–20%).

The geochemical composition of eight granitoid samples from the Kuh-e Sarhangi region was investigated for major and trace element composition analyses (see Table 1; for analytical details, see Appendix A). All the studied samples show acidic compositions (SiO₂ ranging 72.60–76.35 wt%), Al₂O₃ ranging 11.63–13.08 wt% and low Mg# (molar $Mg/[Mg + Fe_{tot}] = 7–35$), with up to ca. 8% alkalis content (Na₂O and K₂O average values of 3.17 and 4.47 wt%, respectively) (Table 2). On the total alkalis vs. silica (TAS) diagram (Le Maitre, 2002), samples plot in the sub-alkaline rhyolite field (Fig. 7A). Based on modal mineralogy, and according to Streckeisen and Le Maitre (1979), the Kuh-e Sarhangi granitoids can be classified as syenogranites and alkali feldspar granites. Samples are dominantly high K/calc/alkaline (Fig. 7B). They also

Table 2

Major and trace element compositions of the Kuh Sarhanghi magmatic rocks.

Locality	Yakhab		Lackbarghashi		Deh Zaman			Robat
Sample	Y1	Y2	Lakh-1	Lakh-2	DZM	DZW	264	R1
<i>Major elements (wt%)</i>								
SiO ₂	75.02	74.46	75.15	76.35	72.60	75.81	75.54	74.42
Al ₂ O ₃	12.62	12.56	11.69	11.63	13.08	12.28	12.64	12.75
FeO _{TOT}	2.12	2.06	1.54	2.10	2.20	1.33	0.61	2.07
MnO	0.03	0.03	0.03	0.03	0.05	0.01	0.01	0.02
MgO	0.36	0.34	0.46	0.15	0.51	0.64	0.06	0.26
CaO	0.79	1.00	0.41	1.25	1.41	0.35	0.58	0.81
Na ₂ O	3.49	3.55	3.16	3.64	3.57	0.51	3.95	3.50
K ₂ O	3.76	3.95	4.45	3.03	4.17	8.38	4.40	3.66
TiO ₂	0.15	0.15	0.11	0.13	0.25	0.13	0.17	0.21
P ₂ O ₅	0.04	0.06	0.03	0.03	0.07	0.02	0.01	0.05
LOI	0.69	0.71	0.89	0.61	0.82	1.02	0.58	0.92
Total (wt%)	99.08	98.85	97.93	98.95	98.72	100.50	98.55	98.67
Mg#	0.16	0.15	0.25	0.07	0.20	0.35	0.10	0.12
A/CNK	1.12	1.05	1.09	1.01	1.01	1.16	1.03	1.14
<i>Trace elements (ppm)</i>								
Sc	12	11	6	7	5	2	2	6
Be	2	2	2	2	2	2	2	2
V	13	10	9	<5	21	6	<5	14
Cr	140	<20	<20	100	<20	60	<20	90
Co	2	2	1	<1	2	1	<1	2
Ni	<20	<20	<20	<20	<20	<20	<20	<20
Cu	<10	<10	<10	10	<10	10	<10	<10
Zn	50	60	<30	50	<30	<30	<30	40
Ga	18	18	17	19	16	15	15	17
Ge	1.8	1.8	1.4	1.9	1.4	1.4	1.4	1.7
As	<5	<5	<5	<5	<5	<5	<5	<5
Rb	117	125	83	107	115	179	86	119
Sr	91	84	88	65	163	66	108	91
Y	29.6	37	55	51.6	27	15.1	19.6	30.6
Zr	151	145	152	186	191	212	188	208
Nb	8.9	8.9	9.2	9.3	7	6	9.6	8.3
Mo	<2	<2	<2	<2	<2	<2	<2	<2
Ag	0.7	0.6	0.6	0.9	0.7	0.9	0.9	0.9
In	<0.1	<0.1	<0.1	<0.1	<0.1	<0.1	<0.1	<0.1
Sn	4	3	3	3	2	9	1	3
Sb	<0.2	<0.2	<0.2	<0.2	<0.2	<0.2	<0.2	<0.2
Cs	1.9	2.1	0.5	2.1	1.7	1.1	0.3	3
Ba	769	712	1986	789	785	926	909	927
La	23.9	31.8	30.5	34.6	18.1	15.7	15	44.4
Ce	52.8	66.7	65.2	72.7	36.9	29.7	26.5	88.1
Pr	6.12	7.69	7.74	8.6	3.79	3.11	2.59	9.46
Nd	24.3	30.1	31.1	34.5	13.9	11.3	9.81	35.2
Sm	5.66	6.79	7.5	7.79	3.01	2.11	2.51	6.63
Eu	0.551	0.631	0.706	1.04	0.531	0.285	0.648	1.05
Gd	5.22	6.32	7.57	7.44	3.13	1.94	2.65	5.55
Tb	0.88	1.05	1.4	1.35	0.6	0.36	0.51	0.89
Dy	5.32	6.28	9.07	8.57	4.03	2.36	3.32	5.24
Ho	1.05	1.26	1.9	1.76	0.85	0.51	0.68	1.05
Er	2.98	3.59	5.76	5.22	2.62	1.59	2.02	3.01
Tm	0.453	0.529	0.861	0.782	0.416	0.259	0.322	0.464
Yb	2.92	3.43	5.64	5.27	2.93	1.85	2.3	3.08
Lu	0.477	0.545	0.917	0.863	0.499	0.319	0.4	0.489
Hf	4.8	4.6	5.4	5.7	5.1	7	5.5	6
Ta	0.72	0.75	0.9	0.79	0.79	0.8	1.55	0.73
W	5.1	<0.5	<0.5	1.1	<0.5	1.3	<0.5	<0.5
Tl	0.43	0.48	0.29	0.37	0.29	0.23	0.14	0.37
Pb	13	22	25	10	18	10	<5	10
Bi	0.1	<0.1	0.1	0.3	<0.1	<0.1	<0.1	<0.1
Th	13.3	13.9	16.4	12.5	15	23.5	19.8	17
U	2.36	2.48	3.11	2.72	3.16	2.27	1.55	2.48
(La/Sm) _N	2.73	3.02	2.63	2.87	3.88	4.80	3.86	4.32
(Dy/Yb) _N	1.22	1.23	1.08	1.09	0.92	0.85	0.97	1.14
(La/Yb) _N	5.87	6.65	3.88	4.71	4.43	6.09	4.68	10.34
Eu*	0.31	0.29	0.29	0.42	0.53	0.43	0.77	0.53
T _{Zr} (°C)	793	783	792	803	800	828	804	823

Note: LOI, loss on ignition; A/CNK, molar Al₂O₃/[(CaO + Na₂O + K₂O)]; Mg#, (molar [Mg]/([Mg] + Fe_{tot})); Eu*, Eu_N/[Sm_N × Gd_N]^{1/2}; T_{Zr} (°C), Zr saturation thermometry (Watson and Harrison, 1983).

show A/CNK (molar Al₂O₃/[CaO + Na₂O + K₂O]) values between 1.00 and 1.16, showing a slight peraluminous signature (mean A/CNK = 1.08). In chondrite normalised diagrams, all samples show

fractionated rare earth elements (REE) patterns, moderately enriched in light REE (LREE) with respect to heavy REE (HREE), with (La/Sm)_N and (La/Yb)_N 2.62 4.80 and 3.87 10.34,

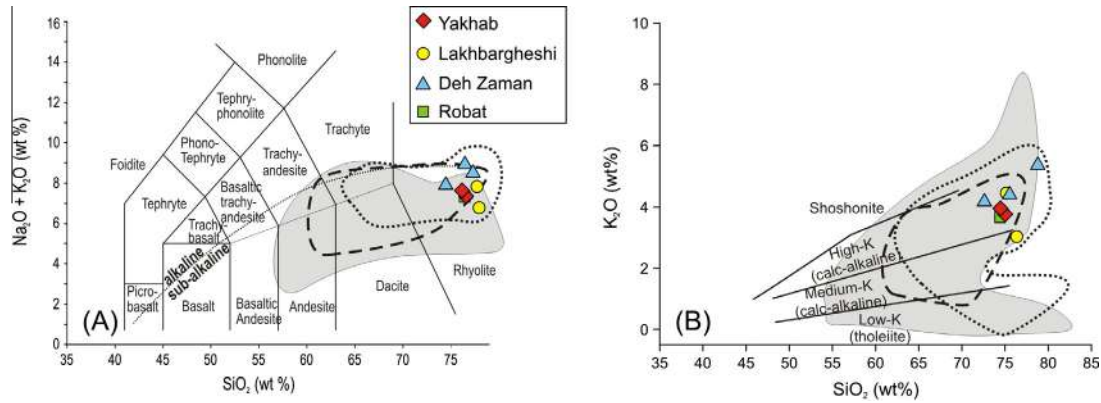


Fig. 7. TAS diagram (sample compositions recalculated on anhydrous basis, with major elements normalised to 100 wt%; after Le Maitre, 2002) for the Kuh-e-Sarhangi granitoids. (B) Plot of K_2O vs. SiO_2 (Peccerillo and Taylor, 1976) with subdivision of volcanic series in shoshonite, high-K, medium-K and low-K and TAS based names of rocks of the subalkaline series. Distribution of the Cadomian Arc magmatism in Iran is also included for comparison: grey field, Chahjam-Biarjmand granitoids (Shafaii Moghadam et al., in press), dotted field, Saghand granitoids (Ramezani and Tucker, 2003), dashed field, granitoids from Soursat Complex (Jamshidi Badr et al., 2013).

respectively. The Eu anomaly ($Eu_N / [(Sm_N \times Gd_N)^{1/2}]$) is systematically negative (Fig. 8A; Table 2). In Primordial Mantle (PM) normalised multi element diagram, all samples are enriched in incompatible elements (LILE, HFSE, and actinides) and depleted in HREE, with a relative depletion in Ti. All samples show distinct negative Nb, Sr and Ti and positive LREE (La, Ce, Nd and Sm) and HFSE (Hf and Zr) anomalies (Fig. 8B) that, together with a low Sr/Y and (La/Yb)_N ratios (Fig. 8C and D), are characteristic features of calc alkaline arc lavas (Defant and Drummond, 1990; Martin, 1999). Tectonomagmatic discrimination diagrams (Nb Y and Rb [Y + Nb], Pearce et al., 1984) confirm a volcanic arc setting (Fig. 8E). Finally, the Kuh e Sarhangi granites show Zr in the range 145–212 ppm, and application of Zr saturation thermometry (Watson and Harrison, 1983) produced a T window of zircon saturation in melt at 782–828 °C with a mean value of 803 °C (Table 2).

5. Thermobarometry

In order to provide constraints on the thermobaric environment associated with pluton crystallisation and emplacement in the Kuh e Sarhangi region, we focus our investigations on the Lakhbargheshi body, where a well defined (about hundreds metre thick) thermal aureole has been recognised in the field. Inverse modelling thermobarometry (*cf.* Powell and Holland, 2008) was firstly adopted in order to assess climax of contact metamorphism based on mineralogical assemblages and compositions of selected host rock samples collected from ca. 300 to 50 m away to the granite, along a path nearly orthogonal to the regional foliation (samples 855, 854 and 17, respectively; Fig. 2 and Table 1; for analytical details see Appendix A). Calculations were performed by using the THERMOCALC software (3.26 version) and its internally consistent thermodynamic data set (Powell and Holland, 2008) in the average P – T calculation mode (multiequilibrium thermobarometry). Mineral formula recalculations and data activities have been calculated through the AX2000 program enclosed in the THERMOCALC package. Average pressure and temperature estimates are expressed together with their uncertainties ($\pm 1\sigma$) and the relative correlation coefficient (cor) as a 95% confidence ellipse. We only considered consistent calculations, as expressed by the 'sigfit' coefficient (Powell and Holland, 1994). Results from inverse thermobarometry were then integrated with those obtained from P – T – X (forward) pseudosection modelling by applying the Perple_X_07 software (Connolly, 2005; <http://www.perplex.ethz.ch>, v. 6.6.9) with the aim to constrain crystallisation

conditions of the Kuh e Sarhangi granitoids by modelling the P – T stability of the suprasolidus primary igneous assemblage.

5.1. Multiequilibrium thermobarometry

The peak mineralogical assemblage in the proximal contact zone of the Lakhbargheshi pluton consists of Grt Ms Pl Qz Ep \pm Amp. Equilibrium textures are commonly observed at the thin section scale. Garnet porphyroblasts are typically poikiloblastic, hosting multiphase inclusions made of Qz Pl Ep Am Ilm (Fig. 9A D). Late stage Bt Chl aggregates are observed to rim the Amp Grt assemblage, often in association with the texturally late Pa and Ab. The garnet composition (see Appendix A for analytical details) is Alm rich and chemical profiles show bell shaped decrease of Sps from core to rim, associated with Pyr increase (core to rim: Alm_{52–71}Grs_{27–18}Pyr_{04–10}Sps_{19–02}; Fig. 9E, top) which is a typical effect of prograde zoning (e.g., Spear, 1993). Amphibole shows tschermakite compositions (Leake et al., 2004), with X_{Mg} in the range 0.31–0.38, $Al_2O_3 = 15.80–16.98$ wt% and $TiO_2 = 0.37–0.42$ wt%. No chemical zoning was observed moving from the core to the rim domains within the same crystals (Fig. 9E, bottom). Primary K white mica is rich in the muscovite component (Ms_{60–63}Pa_{17–23}Cel_{18–22}; Si⁴⁺ 3.11–3.15, Na = 0.17–0.23); secondary white mica is instead Pa (Ms_{08–13}Pa_{83–96}). Primary feldspar consists of oligoclase plagioclase (An_{16–18}Ab_{81–84}Or_{0–1}), whereas late plagioclase consists of Ab. No chemical zoning is evident in either type of feldspars. Epidote has pistacite compositions ($XP_s = [Fe^{3+} / (Fe^{3+} + Al)] \times 100$) ranging 18–26%, with the higher X_{Ps} contents for epidote grain found in the matrix assemblage. Combining the Grt rim compositions with those of the assemblage made of Ms Pl Ep Qz for the metapelites and Pl Ep Qz Amp for the metabasite, respectively, THERMOCALC outputs constrain the metamorphic conditions in the thermal aureole of the Lakhbargheshi body in the P – T window of 590–680 °C and 10–12 kbar (Fig. 10; Table 3).

5.2. Forward modelling thermobarometry

Pseudosections in the NCKFMASmHTO (Na_2O – K_2O – CaO – FeO – MgO – Al_2O_3 – SiO_2 – MnO – H_2O – TiO_2 – O_2) chemical system were calculated for the composition of sample Lakh 1 (Table 2). The sample was chosen as representative of the Kuh e Sarhangi granitoid suite, since it (i) shows only minor effects of solid state textural and mineralogical overprint metamorphic re-equilibration; and (ii) it contains epidote and Grs rich garnet as constituents of the

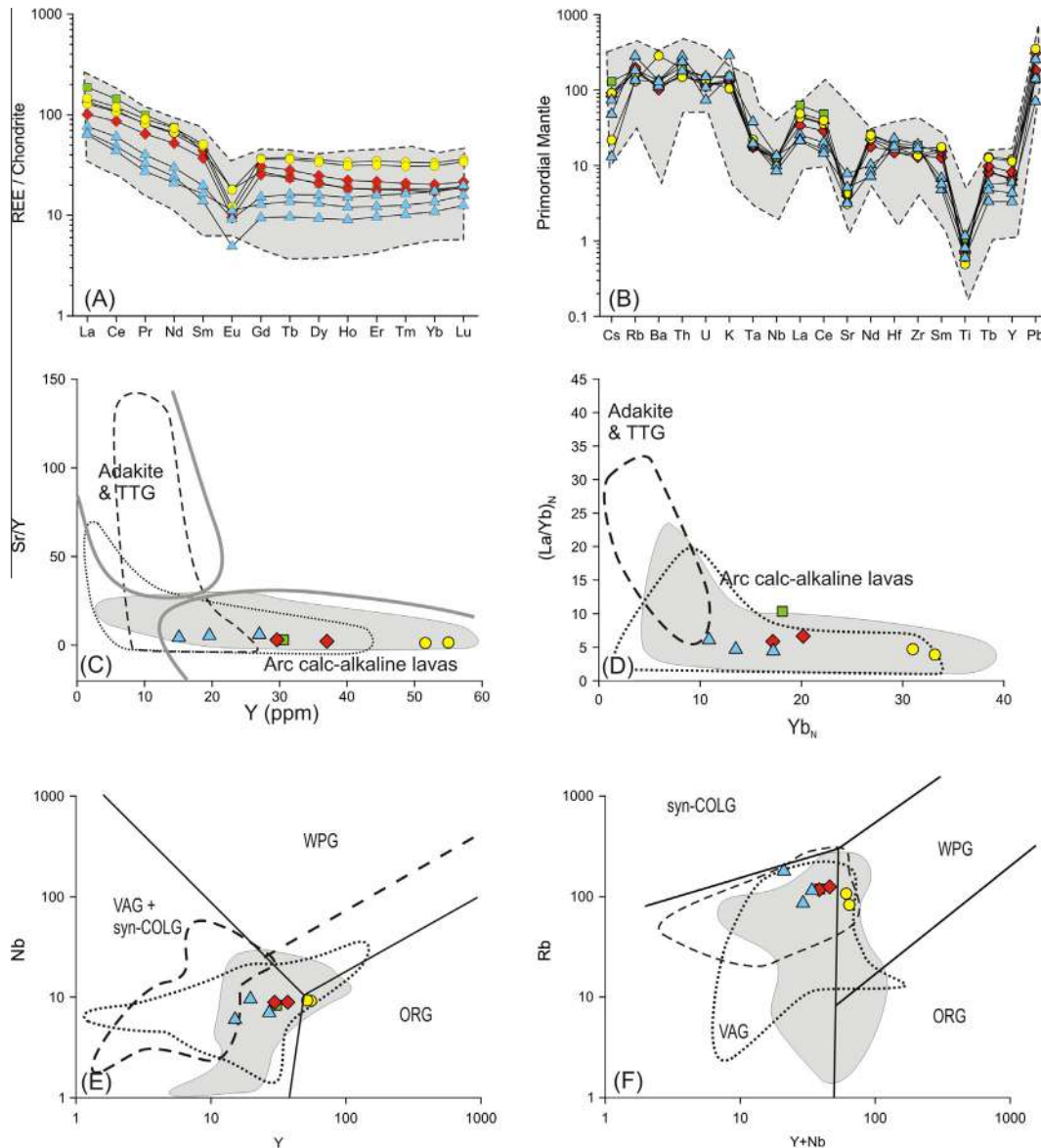


Fig. 8. (A) Chondrite- and (B) primitive mantle-normalized trace element variation diagrams for the Kuh-e-Sarhangi granitoids. Normalizing values are from Sun and McDonough (1989). The grey field plot the cumulative data set available from the Cadomian arc magmatism in Iran (after Ramezani and Tucker, 2003; Jamshidi Badr et al., 2013; Shafaii Moghadam et al., in press). The Kuh-e-Sarhangi granitoids plotted in the Sr/Y vs. Y (C) and chondrite-normalized La/Yb ratio vs. Yb (D). Fields of adakite and TTG and arc calc-alkaline lavas are after Defant and Drummond (1990) and Martin (1999). (E and F) The Kuh-e-Sarhangi granitoids plotted in discrimination diagrams for granitic rocks (Pearce et al., 1984) showing the fields of ocean ridge (OR), volcanic arc (VA), syn-collisional (SC), and within-plate (WP) granitic rocks. Symbols as in Fig. 7.

primary igneous mineral assemblage, attesting for the deepest conditions of magma crystallisation/emplacement (cfr. Harangi et al., 2001; Schmidt and Poli, 2004). The following solid solution mixing models offered by Perple_X were considered in the calculations (details in solut.dat; PERPLEX 07; database: hp04ver.dat): Ep(HP) for epidote, Pheng (HP) for white mica, feldspar for feldspar, TiBio(HP) for biotite, Gt(HP) for garnet, and melt(HP) for the melt phase. The H₂O content was fixed to 3 wt% in order to model wet conditions, whereas O₂ was fixed at 0.05 wt%, equivalent to ca. 20 wt% of total FeO being Fe₂O₃. Results show that stability of the Ep bearing igneous assemblage made of Qz Fsp Gt Bt in suprasolidus conditions occurs in a narrow field near the solidus, at a minimum pressure of 9–10 kbar and 600–620 °C (dark grey field in Fig. 10). It is worth nothing that the calculated Grs iso plots (orange dashed lines in Fig. 10) for the Lakhbargheshi granite (X_{Ca} = 0.35–0.45) are compatible with the stability of magmatic

epidote. This evidence constrains garnet crystallisation close to the solidus conditions. These results are in good agreement with those obtained from metamorphic thermobarometry, and collectively constrain pluton emplacement/crystallisation in a thermobaric environment compatible with the upper pressure field of the amphibolite facies (Fig. 10).

The absence of epidote in equilibrium with garnet in the primary magmatic assemblage and the lower grade conditions of the host rocks in the Deh Zaman (ca. 3–4 kbar and 500–550 °C as constrained by the staurolite and andalusite stability in the KFMASH compositional system; Bucher and Frey, 2002) and Yakab/Robat areas suggest lower pressure conditions of crystallisation/emplacement for the Deh Zaman and Yakhab/Robat plutons. Nevertheless, taking into account the comparable Zr saturation thermometry across the samples (ca. 800 °C; Table 2), a similar melt extraction history can be proposed.

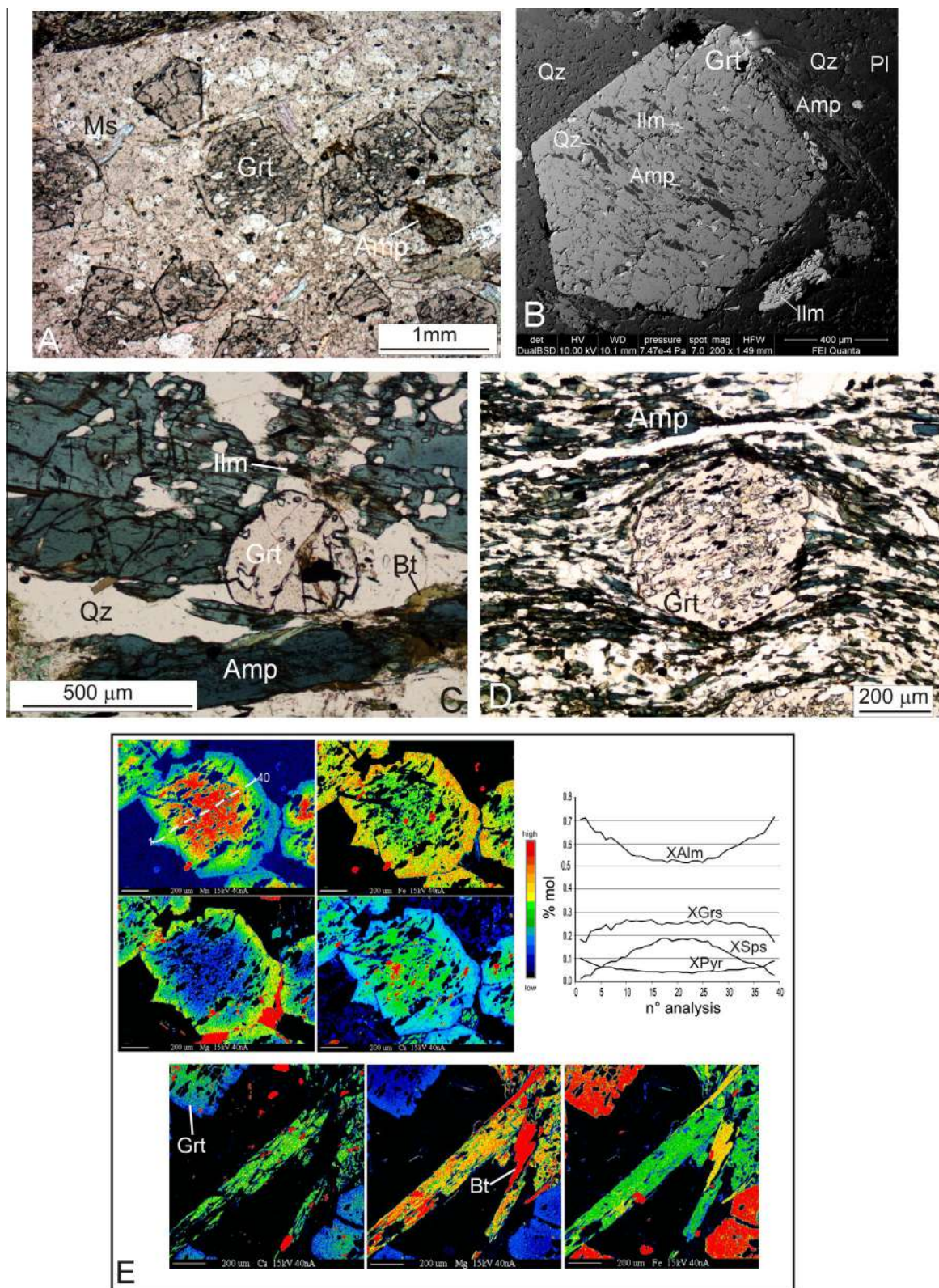


Fig. 9. Microtexture of the amphibolite-facies host rocks of the Lakhbargheshi body. (A) Poikiloblastic, euhedral garnet (Grt) porphyroblasts in textural equilibrium with K-white mica (Ms) and Ca-amphibole (Amp) in a quartz-plagioclase matrix (sample 855; natural light). (B) Backscattered electron (BSE) image showing the inclusion assemblage in a garnet porphyroblast (sample 855). (C) Equilibrium texture among garnet (Grt), Ca-amphibole (Amp) and ilmenite (Ilm) (sample 17, natural light). (D) Syn-kinematic growth of garnet porphyroblast with curved inclusion trails in an amphibole-plagioclase matrix. The inclusion assemblage in garnet consists of quartz and ilmenite (dark grains) (sample 854; natural light). (E) Representative qualitative compositional map and quantitative EMPA profiles showing variation in cation distribution in garnets (top; cations: Mg, Fe, Ca, Mn) and amphibole (bottom; cation: Ca, Fe, Mg) from the amphibolite country rocks (sample 855).

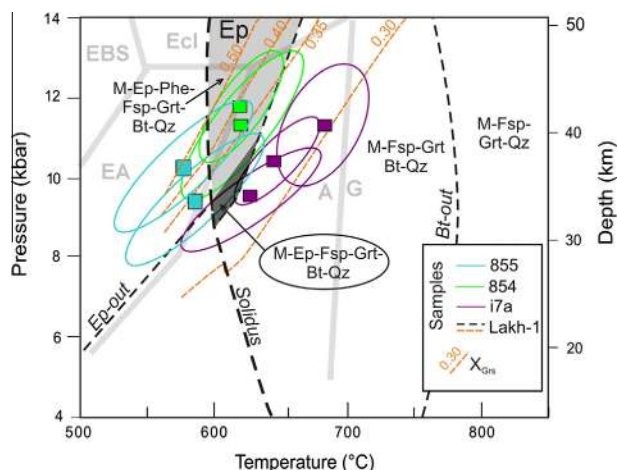


Fig. 10. Results from multiequilibrium thermobarometry as obtained from the THERMOCALC software in the average P - T calculation mode applied to the metamorphic country rocks of the Lakhbargheshi body. Representative average P - T results are shown with error quoted at 1σ level (coloured ellipses). The grid also shows the stability fields of the magmatic (coexisting with melt, M) assemblage epidote (Ep), biotite (Bt), garnet (Grt), feldspar (Fsp), quartz (Qtz), biotite, epidote and the solidus curve as obtained from P - T - X pseudosection modeling (by using the Perple_X07 software) in the system NKFMAHSMnTO with a bulk composition (wt%) Na_2O 3.64, K_2O 3.03, FeO 2.10, MgO 0.15, Al_2O_3 11.63, SiO_2 76.35, H_2O 3.00, MnO 0.03, TiO_2 0.13, O_2 0.05 (sample Lakh-1). The light grey area indicates the stability of magmatic Ep, whereas the dark grey area indicates the stability field of the magmatic assemblage Ep-Fsp-Qz-Grt-Bt in coexistence with melt (M). The metamorphic facies fields are after Bucher and Frey (2002); A, amphibolite facies; E, eclogite facies, EA, epidote amphibolite facies; G, granulite facies.

6. LA-SF-ICPMS U-Pb zircon geochronology

The geochronology of the Kuh e Sarhangi magmatism was assessed through LA ICPMS U-Pb zircon geochronology. A list of the analysed samples is shown in Table 1; their petrographical description is provided in the Appendix B. After separation, zircon grains were investigated by means of backscattered electron (BSE) and cathodoluminescence (CL) imaging. Selected spots of 23–33 μm in diameter were then analysed for U, and Pb isotopic compositions by laser ablation sector field inductively coupled plasma mass spectrometry (LA-SF-ICPMS) at Goethe University Frankfurt (cfr. Gerdes and Zeh, 2006, 2009). Details of the analytical protocols are provided in the Appendix A. Analytical results are shown in Table 4. Age calculations and graphical display were

obtained using the computer program ISOPLOT ver. 3.0 (Ludwig, 2003) and are shown in Fig. 11.

Deh Zaman Two samples were analysed in this study, sample DZM and DZW, corresponding to the melanocratic and felsic portions of the Deh Zaman composite body as recognised in the field (Fig. 3A). Zircon separates from sample DSM usually consist of elongated prismatic crystals (300–450 \times 100–150 μm). They appear as moderately to high luminescent at the CL imaging, with characteristic growth banding, oscillatory and sector zoning textures. In BSE imaging, the crystals typically show nearly uniform growth zoning, usually associated with brighter inner domains. Oscillatory zoned zircon cores and rims have variable Th/U ratios (0.3–2.3) with a mean value of 0.75 ($n = 22$). Age analyses reveal apparent $^{206}\text{Pb}/^{238}\text{U}$ ages spanning from c. 516 to 664 Ma. A population of ten analyses with U/Th ranging 0.41–0.91 form a

concordant cluster with a Concordia age of 557 ± 4 Ma (2σ , MSWD (of concordance) = 0.47) (Fig. 11A, top). Zircon separates from sample DSW also show dominant elongated prismatic shapes (200

300 \times 100–150 μm). At the CL imaging, they appear as dark luminescent with prominent growth oscillatory or sector zoning. Often, the grains show corroded rims in association with irregular, highly luminescent alteration zones that locally penetrate the crystal cores with convolute zoning patterns. In BSE images, oscillatory growth zoning usually is usually preserved. Oscillatory zoned zircon cores and rims have Th/U ratios ranging 0.55–2.30, while the high luminescent alteration zones shows more scattered ratios spanning 0.55–4.31. Age analyses reveal apparent $^{206}\text{Pb}/^{238}\text{U}$ ages spanning from c. 233 to 651 Ma ($n = 36$). A population of thirteen analyses of oscillatory zoned domains, with U/Th ranging 0.61–1.44,

define a concordant cluster with a Concordia age of 561 ± 3 Ma (2σ , MSWD (of concordance) = 0.21) (Fig. 11A, bottom).

Lakhbargheshi The zircon separates from sample Lakh 1 consist of elongated (250–450 \times 75–150 μm) prismatic crystals. CL images show homogenous cores with luminescent oscillatory and planar growth zones, only rarely affected by bright alteration over growth in the rims domains of a few grains. BSE images show nearly homogeneous growth zoning. Zircon cores and rims have nearly uniform Th/U ratios ranging 0.56 to 89. Age analyses reveal apparent $^{206}\text{Pb}/^{238}\text{U}$ ages spanning from c. 461 to 531 Ma ($n = 17$). A population of eight analyses of oscillatory zoned domains, with U/Th ranging 0.69–0.89, form a concordant cluster with a Concordia age of 536 ± 5 Ma (2σ , MSWD (of concordance and equivalence, $C + E$) = 0.36) (Fig. 11B).

Yakhab The zircon separates from sample Y1 consist of prismatic (200–300 \times 75–150 μm) and stubby crystals. They show dark luminescent cores and rims, with oscillatory zoning, with only

Table 3
Representative results of THERMOCALCv.3.26 average P - T calculations (all uncertainties are given at the 1-sigma level).

Locality	Sample	Assemblage	Independent set of reactions	avT	sd(T)	avP	sd(P)	corr	Note
Lakhbargheshi	855	py, gr, alm, tr, fact, ts, parg, gl, an, ab, cz, q, H_2O	11, 12, 13, 14	588	44	10.3	1.3	0.867	gl, parg, ab excluded
			11, 12, 13, 14	566	60	12.3	2	0.813	gl, parg, ab excluded
	854	py, gr, alm, spss, phl, ann, east, mu, cel, fcel, pa, an, ab, q, H_2O	2, 3, 4, 5, 6	618	37	11.5	1.5	0.815	east excluded
			2, 3, 4, 5, 6	617	25	12	1.1	0.803	east excluded
	i7a	py, gr, alm, spss, cs, ep, phl, ann, east, mu, cel, fcel, pa, an, ab, q, H_2O	1, 2, 3, 4, 8, 9, 10	645	26	10.6	0.9	0.806	all phases considered 0.439
			4, 6, 7, 8, 9	679	29	11.5	1.3	0.856	east, an excluded
			2, 3, 4, 6, 8	625	44	9.7	1.1		east, pa excluded

(1) $\text{phl} + \text{east} + 6\text{q} = \text{py} + 2\text{cel}$; (2) $2\text{ann} + \text{mu} + 6\text{q} = \text{alm} + 3\text{fcel}$; (3) $\text{phl} + 3\text{an} = \text{py} + \text{gr} + \text{mu}$; (4) $\text{ann} + 3\text{an} = \text{gr} + \text{alm} + \text{mu}$; (5) $\text{py} + 3\text{ann} + 2\text{pa} + 9\text{q} = 3\text{alm} + 3\text{cel} + 2\text{ab} + 2\text{H}_2\text{O}$; (6) $\text{mu} + 2\text{phl} + 6\text{q} = \text{py} + 3\text{cel}$; (7) $\text{py} + \text{ann} = \text{alm} + \text{phl}$; (8) $5\text{py} + 15\text{ann} + 12\text{cz} + 33\text{q} = 8\text{gr} + 15\text{alm} + 15\text{cel} + 6\text{H}_2\text{O}$; (9) $6\text{ab} + 4\text{phl} + 12\text{cz} = 3\text{py} + 8\text{gr} + \text{mu} + 3\text{cel} + 6\text{pa}$; (10) $3\text{east} + 6\text{q} = \text{py} + \text{phl} + 2\text{mu}$; (11) $10\text{py} + 3\text{tr} + 24\text{cz} = 4\text{gr} + 15\text{ts} + 12\text{an}$; (12) $2\text{py} + 4\text{gr} + 3\text{ts} + 12\text{q} = 3\text{tr} + 12\text{an}$; (13) $19\text{ts} = 14\text{py} + 3\text{tr} + 16\text{cz} + 8\text{H}_2\text{O}$; (14) $5\text{py} + 3\text{fact} = 5\text{alm} + 3\text{tr}$.

Table 4
Zircon LAICMPS U–Pb data from the Kuh-e-Sarhangi granitoid rocks.

Sample/spot	²⁰⁷ Pb ^a (cps)	U ^b (ppm)	Pb ^b (ppm)	Th ^b U	²⁰⁶ Pb/ ²³⁸ U ^c (%)	²⁰⁶ Pb ^d ²³⁸ U	±2σ (%)	²⁰⁷ Pb ^d ²³⁵ U	±2σ (%)	²⁰⁷ Pb ^d ²⁰⁶ Pb	±2σ (%)	rho ^e	²⁰⁶ Pb ²³⁸ U	±2σ (Ma)	²⁰⁷ Pb ²³⁵ U	±2σ (Ma)	²⁰⁷ Pb ²⁰⁶ Pb	±2σ (Ma)	Conc. ^f (%)
<i>DZM</i>																			
A04	7146	165	16	0.58	b.d.	0.0877	2.1	0.7166	2.6	0.05926	1.5	0.81	542	11	549	11	577	33	94
A05	1648	33	5	2.30	b.d.	0.09531	2.2	0.7768	3.7	0.05911	3.0	0.60	587	12	584	17	571	64	103
A06	11784	278	28	0.91	0.0	0.08837	1.9	0.7117	2.4	0.05841	1.4	0.80	546	10	546	10	545	32	100
A07	1937	38	4	0.63	0.2	0.08332	3.5	0.655	10.6	0.05701	10.0	0.33	516	17	512	44	492	221	105
A08	5786	130	13	0.74	0.0	0.08992	1.6	0.7332	2.6	0.05914	2.0	0.62	555	9	558	11	572	45	97
A09	7170	169	17	0.78	0.0	0.08649	2.3	0.6799	2.8	0.05702	1.5	0.84	535	12	527	11	492	34	109
A10	4788	72	7	0.63	4.4	0.08786	3.3	0.7041	7.8	0.05812	7.0	0.43	543	17	541	33	534	154	102
A11	5405	125	12	0.54	0.1	0.08981	2.6	0.7348	3.9	0.05934	3.0	0.66	554	14	559	17	580	64	96
A12	12780	309	31	0.74	0.0	0.08976	1.9	0.7288	2.4	0.05888	1.5	0.79	554	10	556	11	563	33	98
A13	3161	74	7	0.79	0.6	0.08684	2.6	0.7146	5.9	0.05969	5.3	0.43	537	13	548	25	592	116	91
A14	11132	250	24	0.69	0.1	0.08505	2.6	0.6765	3.3	0.05769	2.0	0.79	526	13	525	14	518	44	102
A15	15717	312	31	0.66	0.5	0.09039	2.9	0.7312	4.4	0.05867	3.3	0.66	558	16	557	19	555	72	101
A17	17191	385	42	1.08	0.8	0.09128	2.8	0.6496	5.1	0.05161	4.3	0.54	563	15	508	21	268	99	210
A18	11821	280	29	0.88	0.0	0.09261	2.7	0.7549	3.7	0.05912	2.5	0.74	571	15	571	16	572	54	100
A19	10429	240	25	0.78	b.d.	0.09304	2.7	0.7575	3.3	0.05905	1.9	0.82	573	15	573	14	569	41	101
A20	12780	281	28	0.68	0.0	0.09191	3.0	0.7433	3.6	0.05866	1.9	0.85	567	16	564	16	554	41	102
A21	11168	228	21	0.41	1.1	0.09151	1.8	0.7348	3.3	0.05823	2.8	0.55	564	10	559	14	538	61	105
A22	7193	162	18	0.35	0.1	0.1086	2.8	0.9323	3.8	0.06229	2.6	0.74	664	18	669	19	684	55	97
A23	6084	132	13	0.64	0.4	0.08951	2.7	0.7223	3.5	0.05853	2.3	0.76	553	14	552	15	550	50	101
A26	39107	889	83	0.55	0.0	0.08776	1.9	0.7061	2.2	0.05835	1.1	0.88	542	10	542	9	543	23	100
A27	5510	112	11	0.52	2.0	0.08904	2.5	0.7181	4.9	0.0585	4.2	0.51	550	13	550	21	548	92	100
A28	12605	290	26	0.59	0.0	0.08468	1.9	0.6813	2.3	0.05835	1.4	0.80	524	9	528	10	543	31	97
<i>Lakh-1</i>																			
g24	560006	3227	340	0.89	2.5	0.08746	2.3	0.7071	4.3	0.0586	3.6	0.53	541	12	543	18	553	79	98
g25	126194	713	70	0.85	b.d.	0.08703	2.6	0.6943	3.2	0.0579	1.9	0.80	538	13	535	13	525	42	103
g26	42622	238	22	0.69	0.1	0.08534	2.3	0.6842	4.0	0.0582	3.3	0.57	528	12	529	17	535	72	99
g27	8163	55	4.3	0.34	1.0	0.0741	3.6	0.576	6.9	0.0564	5.9	0.53	461	16	462	26	467	130	99
g28	20637	126	12	0.73	b.d.	0.08664	2.1	0.6823	4.3	0.0571	3.8	0.48	536	11	528	18	496	84	108
g29	35287	194	19	0.85	0.5	0.08614	2.2	0.6808	4.3	0.0573	3.7	0.51	533	11	527	18	504	82	106
g30	9907	53	4.8	0.75	0.7	0.07767	2.4	0.596	11	0.0557	11	0.22	482	11	475	42	440	235	110
g31	39449	212	21	0.94	0.0	0.08366	2.0	0.6675	4.9	0.0579	4.5	0.40	518	10	519	20	525	99	99
g32	30672	158	15	0.71	0.7	0.08395	2.0	0.6668	3.9	0.0576	3.3	0.52	520	10	519	16	515	72	101
g36	53017	299	30	0.80	0.1	0.08657	2.9	0.6929	3.8	0.0581	2.5	0.76	535	15	535	16	532	55	101
g37	57652	309	30	0.75	0.4	0.08678	2.6	0.693	4.7	0.0579	3.9	0.55	536	13	535	20	527	86	102
g38	68778	382	34	0.78	0.2	0.07812	2.1	0.6039	2.8	0.0561	1.9	0.75	485	10	480	11	455	41	107
g39	19731	109	10	0.56	0.1	0.08755	3.2	0.7207	7.2	0.0597	6.5	0.44	541	16	551	31	593	140	91
g40	39684	206	21	0.86	0.1	0.08653	3.7	0.6813	4.4	0.0571	2.4	0.84	535	19	528	18	496	53	108
g41	33177	183	18	0.69	0.3	0.08752	4.8	0.7098	6.1	0.0588	3.6	0.80	541	25	545	26	560	79	97
g42	44532	244	24	0.81	0.2	0.08772	4.6	0.7113	6.1	0.0588	4.1	0.75	542	24	545	26	560	89	97
g43	54978	283	28	1.01	0.5	0.08362	4.3	0.6635	5.3	0.0576	3.1	0.80	518	21	517	22	513	69	101
<i>DZW</i>																			
A37	20253	548	53	0.52	b.d.	0.09131	2.2	0.7317	2.7	0.05811	1.6	0.82	563	12	558	12	534	34	105
A38	10768	298	26	0.55	0.80	0.08108	1.8	0.6507	4.4	0.0582	4.0	0.42	503	9	509	18	537	87	94
A39	3748	21	3	1.62	52.3	0.04670	7.3	0.422	30.4	0.06554	29.6	0.24	294	21	357	96	792	620	37
A40	16872	499	50	0.70	0.01	0.08997	2.1	0.7167	2.8	0.05778	1.9	0.73	555	11	549	12	521	42	107
A41	3179	50	4	2.03	18.1	0.03676	5.6	0.2242	34.6	0.04422	34.1	0.16	233	13	205	66	-98	839	-237
A42	10358	282	28	0.61	b.d.	0.09259	1.8	0.7522	2.5	0.05892	1.7	0.74	571	10	569	11	564	36	101
A43	4640	372	37	0.66	0.01	0.08889	2.3	0.7138	3.2	0.05824	2.2	0.72	549	12	547	13	539	48	102
A44	10931	288	29	0.67	0.06	0.09070	1.8	0.733	2.8	0.05861	2.2	0.62	560	9	558	12	553	49	101
A45	17987	1176	143	1.84	b.d.	0.09108	2.9	0.735	3.4	0.05853	1.8	0.85	562	15	559	15	550	39	102
A48	2032	123	13	1.02	b.d.	0.08831	2.2	0.7205	4.3	0.05917	3.7	0.51	546	12	551	19	573	81	95
A49	4195	256	26	0.74	0.12	0.08966	2.0	0.7262	3.6	0.05875	3.0	0.55	554	10	554	15	558	66	99

A50	6776	112	7	0.55	32	0.03672	3.9	0.2748	30.9	0.05428	30.6	0.13	232	9	247	70	383	688	61
A51	12353	555	36	0.79	0.41	0.05291	2.6	0.3999	4.3	0.05482	3.4	0.61	332	9	342	13	405	76	82
A52	5433	228	22	0.74	0.02	0.08481	3.9	0.6676	4.6	0.05709	2.5	0.85	525	20	519	19	495	54	106
A53	13648	491	51	0.79	b.d.	0.09252	2.0	0.7485	2.5	0.05868	1.6	0.79	570	11	567	11	555	34	103
A54	5167	244	25	0.81	0.87	0.09670	2.2	0.7374	6.9	0.05531	6.5	0.32	595	13	561	30	425	145	140
A55	3257	30	6	4.31	17	0.05902	3.6	0.5835	7.1	0.07171	6.0	0.52	370	13	467	27	978	123	38
A56	1672	33	6	4.13	2.2	0.09272	2.2	0.7497	3.5	0.05864	2.7	0.64	572	12	568	15	554	58	103
A57	5298	331	32	0.73	b.d.	0.08559	2.2	0.6856	2.8	0.05809	1.7	0.80	529	11	530	11	533	37	99
A58	19159	490	48	0.68	b.d.	0.08922	1.9	0.7258	2.4	0.05901	1.5	0.78	551	10	554	10	567	33	97
A59	10792	294	29	0.53	0.05	0.09289	2.0	0.7563	2.5	0.05905	1.5	0.80	573	11	572	11	569	32	101
A60	22206	651	73	0.50	b.d.	0.10620	3.2	0.8898	3.9	0.06076	2.3	0.80	651	20	646	19	631	50	103
A61	12514	336	34	0.59	b.d.	0.09216	2.2	0.7439	2.8	0.05854	1.6	0.81	568	12	565	12	550	35	103
A62	9657	252	25	0.56	b.d.	0.09269	2.0	0.7472	2.6	0.05846	1.7	0.77	571	11	567	11	547	36	104
A63	9888	272	25	0.60	0.52	0.08687	1.8	0.6988	2.6	0.05834	1.9	0.69	537	9	538	11	543	42	99
A64	6375	176	16	0.58	0.01	0.08278	2.0	0.6676	3.0	0.05849	2.3	0.66	513	10	519	12	548	49	94
A65	11183	290	29	0.80	0.08	0.08955	2.2	0.7252	2.9	0.05873	1.9	0.76	553	12	554	13	557	42	99
A66	1607	45	6	2.64	27	0.06342	4.1	0.5712	34.6	0.06532	34.3	0.12	396	16	459	136	785	721	51
A67	2230	73	9	1.44	0.51	0.09093	2.6	0.7313	6.1	0.05833	5.6	0.42	561	14	557	27	542	122	103
A70	8849	330	32	0.55	b.d.	0.08987	2.0	0.73	2.6	0.05891	1.6	0.77	555	10	557	11	564	35	98
A71	7232	261	24	0.55	0.003	0.08496	2.2	0.6879	2.9	0.05872	1.9	0.75	526	11	532	12	557	42	94
A72	15189	491	54	0.82	0.19	0.09503	2.3	0.7786	3.3	0.05942	2.3	0.70	585	13	585	15	583	51	100
A73	15362	433	45	0.57	1.14	0.09361	2.4	0.7604	3.4	0.05892	2.4	0.71	577	13	574	15	564	53	102
A74	2621	104	10	1.04	0.12	0.07967	2.1	0.6486	3.3	0.05904	2.6	0.62	494	10	508	13	569	57	87
A75	10146	372	35	0.61	0.02	0.08605	2.0	0.6916	2.5	0.05829	1.5	0.81	532	10	534	10	541	32	98
A76	12801	499	49	0.68	b.d.	0.08995	2.1	0.7206	2.4	0.05810	1.3	0.85	555	11	551	10	533	28	104

R1

A04	50000	1393	140	0.93	0.1	0.08560	2.4	0.6959	2.9	0.05896	1.5	0.85	529	12	536	12	565	33	94
A05	15789	421	45	0.86	0.05	0.09420	1.9	0.7646	2.9	0.05887	2.1	0.67	580	11	577	13	562	47	103
A06	7802	209	22	0.82	0.30	0.09323	2.0	0.7305	3.2	0.05683	2.6	0.61	575	11	557	14	485	56	119
A07	16923	447	47	0.73	0.63	0.09513	1.9	0.703	3.7	0.0536	3.2	0.51	586	11	541	16	354	72	165
A08	33025	839	92	0.98	0.06	0.09381	2.2	0.7614	3.6	0.05886	2.8	0.61	578	12	575	16	562	62	103
A09	45841	1211	127	1.10	0.02	0.08521	2.3	0.6974	3.0	0.05936	2.0	0.75	527	12	537	13	580	44	91
A10	30054	1530	40	0.46	b.d.	0.02044	4.1	0.1995	5.1	0.07078	3.0	0.81	130	5	185	9	951	61	14
A11	49375	1349	134	0.64	0.06	0.09164	2.0	0.7397	2.6	0.05854	1.6	0.78	565	11	562	11	550	35	103
A12	36821	970	102	0.86	0.1	0.09070	2.1	0.7389	2.8	0.05909	1.8	0.77	560	11	562	12	570	39	98
A13	105318	2711	225	1.07	0.01	0.06579	1.8	0.8127	2.5	0.08959	1.8	0.70	411	7	604	12	1417	35	29
A14	93467	2953	181	1.35	4.5	0.04216	3.6	0.3367	7.5	0.05792	6.6	0.47	266	9	295	19	527	145	51
A15	14252	365	38	0.84	0.07	0.09253	1.7	0.7471	2.7	0.05856	2.1	0.64	570	9	567	12	551	46	104
A16	29516	761	80	0.93	0.02	0.09024	2.2	0.7315	2.4	0.0588	1.0	0.91	557	12	557	10	560	22	100
A17	21762	557	56	1.01	0.47	0.08465	2.5	0.6787	4.1	0.05814	3.2	0.62	524	13	526	17	535	70	98
A19	41677	1060	114	0.84	0.25	0.09488	1.8	0.7616	2.5	0.05821	1.8	0.72	584	10	575	11	538	38	109
A22	61723	2414	229	0.47	0.40	0.09242	2.3	0.7467	4.5	0.0586	3.9	0.50	570	12	566	20	552	86	103
A26	32227	797	78	0.59	0.004	0.08910	2.1	0.7178	2.4	0.05843	1.0	0.90	550	11	549	10	546	22	101
A27	22635	591	64	0.80	0.07	0.09521	2.3	0.7764	2.7	0.05914	1.3	0.88	586	13	583	12	572	28	102
A28	11283	290	29	0.59	b.d.	0.09279	2.3	0.7532	3.0	0.05888	1.9	0.76	572	13	570	13	563	42	102
A29	34789	925	97	0.71	0.07	0.09338	1.8	0.7554	2.3	0.05867	1.4	0.78	576	10	571	10	555	30	104
A30	23118	979	53	0.39	b.d.	0.05004	2.1	0.4440	2.7	0.06436	1.7	0.78	315	7	373	9	753	36	42
A31	18857	513	52	0.70	0.56	0.09281	2.4	0.7593	3.2	0.05934	2.1	0.76	572	13	574	14	579	45	99
A32	36895	946	95	0.62	0.08	0.09184	2.3	0.7436	2.7	0.05872	1.5	0.83	566	12	564	12	557	34	102
A33	8406	176	21	0.57	0.03	0.11220	1.8	0.9442	2.4	0.06104	1.6	0.74	685	12	675	12	641	35	107
A34	32839	878	88	0.80	0.06	0.08907	1.8	0.7384	2.4	0.06012	1.5	0.78	550	10	561	10	608	32	90
A35	27888	692	69	0.58	0.02	0.09247	2.6	0.7509	3.0	0.05889	1.4	0.89	570	14	569	13	563	29	101
A36	27423	724	74	0.71	0.05	0.09340	2.0	0.7567	2.6	0.05876	1.6	0.78	576	11	572	11	558	35	103

Y-1

A29	12172	296	30	0.85	0.1	0.08743	2.0	0.6894	2.9	0.05719	2.1	0.69	540	10	532	12	499	47	108
A32	13391	263	29	0.78	0.1	0.09437	1.9	0.7773	2.8	0.05974	2.1	0.68	581	11	584	13	594	45	98
A33	31302	659	70	0.83	b.d.	0.09212	1.7	0.7542	2.1	0.05938	1.1	0.84	568	9	571	9	581	24	98
A34	12841	298	28	0.55	0.2	0.08887	2.3	0.7287	3.4	0.05947	2.5	0.67	549	12	556	15	584	55	94

(continued on next page)

Table 4 (continued)

Sample/spot	²⁰⁷ Pb ^a (cps)	U ^b (ppm)	Pb ^b (ppm)	Th ^b U	²⁰⁶ Pb ^c (%)	²⁰⁶ Pb ^d ²³⁸ U	±2σ (%)	²⁰⁷ Pb ^d ²³⁵ U	±2σ (%)	²⁰⁷ Pb ^d ²⁰⁶ Pb	±2σ (%)	rho ^e	²⁰⁶ Pb ²³⁸ U	±2σ (Ma)	²⁰⁷ Pb ²³⁵ U	±2σ (Ma)	²⁰⁷ Pb ²⁰⁶ Pb	±2σ (Ma)	Conc. ^f (%)
A35	56346	1269	113	1.63	2.8	0.07051	3.7	0.566	5.2	0.05822	3.7	0.71	439	16	455	19	538	81	82
A36	25758	501	54	0.76	b.d.	0.09574	1.8	0.7842	2.0	0.0594	1.0	0.86	589	10	588	9	582	22	101
A39	33886	1602	137	0.37	0.0	0.08709	4.6	0.7077	4.8	0.05893	1.6	0.95	538	24	543	21	565	34	95
A40	25150	575	57	0.62	0.0	0.09109	1.6	0.7425	2.2	0.05911	1.5	0.72	562	9	564	10	571	33	98
A41	10064	239	24	0.50	0.1	0.09579	2.1	0.7906	2.7	0.05986	1.7	0.77	590	12	591	12	598	37	99
A42	15072	500	49	0.42	0.1	0.09327	2.1	0.7658	2.7	0.05955	1.7	0.78	575	12	577	12	587	37	98
A43	39816	886	80	0.45	0.0	0.08584	2.0	0.7038	2.5	0.05946	1.5	0.79	531	10	541	11	584	33	91
A44	23242	469	49	0.83	0.1	0.09207	1.9	0.74	2.5	0.05829	1.5	0.79	568	11	562	11	541	33	105
A45	15606	289	31	0.73	0.9	0.09304	1.8	0.7616	4.0	0.05937	3.6	0.44	573	10	575	18	581	78	99
A48	46510	1094	93	0.39	0.5	0.08446	1.8	0.6855	3.5	0.05887	3.0	0.51	523	9	530	14	562	65	93
A49	16638	324	31	0.79	1.0	0.08713	3.8	0.6686	12.0	0.05565	11.4	0.31	539	20	520	50	439	254	123
A53	21973	474	52	0.90	0.0	0.09527	1.9	0.7672	2.2	0.05841	1.2	0.85	587	11	578	10	545	25	108
A54	28257	611	63	0.76	0.0	0.0921	1.8	0.7492	2.1	0.059	1.1	0.84	568	10	568	9	567	25	100
A55	13139	638	67	0.67	b.d.	0.09526	1.8	0.7688	2.5	0.05853	1.7	0.73	587	10	579	11	550	38	107
A56	7629	363	37	0.49	0.2	0.09427	1.9	0.7746	2.8	0.05959	2.1	0.68	581	11	582	13	589	45	99
A57	39144	804	84	0.71	b.d.	0.09308	2.0	0.7538	2.2	0.05873	1.1	0.87	574	11	570	10	557	24	103
A58	21159	435	44	0.58	b.d.	0.09352	1.7	0.76	2.0	0.05894	1.2	0.82	576	9	574	9	565	25	102
A61	11396	251	26	0.70	0.3	0.09299	2.2	0.7642	3.4	0.05961	2.6	0.63	573	12	576	15	589	57	97
A62	34748	789	73	0.48	0.0	0.08902	2.1	0.7238	2.6	0.05897	1.5	0.82	550	11	553	11	566	32	97
A63	70726	1827	181	1.36	1.8	0.08361	1.9	0.6734	3.7	0.05841	3.2	0.50	518	9	523	15	545	70	95
A64	8007	222	21	0.59	0.2	0.08911	2.0	0.7313	3.2	0.05952	2.5	0.62	550	11	557	14	586	55	94
A65	48145	1366	142	1.04	0.1	0.08307	2.1	0.6726	4.3	0.05872	3.8	0.48	514	10	522	18	557	83	92
A66	7330	201	21	0.56	b.d.	0.09501	1.8	0.7758	2.7	0.05922	2.0	0.67	585	10	583	12	575	44	102
A67	9334	273	28	0.74	0.1	0.0936	2.0	0.7627	2.5	0.05909	1.6	0.79	577	11	576	11	571	34	101
A68	81871	2578	247	0.96	0.1	0.08919	2.1	0.7299	2.7	0.05936	1.6	0.79	551	11	557	11	580	36	95
A69	10616	306	29	0.35	b.d.	0.09361	2.4	0.7591	2.9	0.05882	1.6	0.83	577	13	574	13	560	35	103
Plesovice ^g	9782	419	21	0.13	0.08	0.05399	1.5	0.3970	2.6	0.05333	1.2	0.63	339	5	339	7	343	27	101
91500 ^g	6831	60	11	0.39	0.25	0.17948	1.0	1.8618	2.3	0.07523	1.8	0.66	1064	9	1068	15	1075	37	99

Spot size = 20 μm; depth of crater ~15 μm. ²⁰⁶Pb/²³⁸U error is the quadratic additions of the within run precision (2 SE) and the external reproducibility (2 SD) of the reference zircon. ²⁰⁷Pb/²⁰⁶Pb error propagation (²⁰⁷Pb signal dependent) following Gerdes and Zeh (2009). ²⁰⁷Pb/²³⁵U error is the quadratic addition of the ²⁰⁷Pb/²⁰⁶Pb and ²⁰⁶Pb/²³⁸U uncertainty.

^a Within run background-corrected mean ²⁰⁷Pb signal in cps (counts per second).

^b U and Pb content and Th/U ratio were calculated relative to GJ-1 reference zircon.

^c Percentage of the common Pb on the ²⁰⁶Pb. b.d. = below detection limit.

^d Corrected for background, within-run Pb/U fractionation (in case of ²⁰⁶Pb/²³⁸U) and common Pb using Stacey and Kramers (1975) model Pb composition and subsequently normalised to GJ-1 (ID-TIMS value/measured value); ²⁰⁷Pb/²³⁵U calculated using ²⁰⁷Pb/²⁰⁶Pb/(²³⁸U/²⁰⁶Pb*1/137.88).

^e rho is the ²⁰⁶Pb/²³⁸U/²⁰⁷Pb/²³⁵U error correlation coefficient.

^f Degree of concordance = ²⁰⁶Pb/²³⁸U age/²⁰⁷Pb/²⁰⁶Pb age × 100.

^g Accuracy and reproducibility was checked by repeated analyses (n = 8) of reference zircon Plesovice and 91500; data given as mean with 2 standard deviation uncertainties.

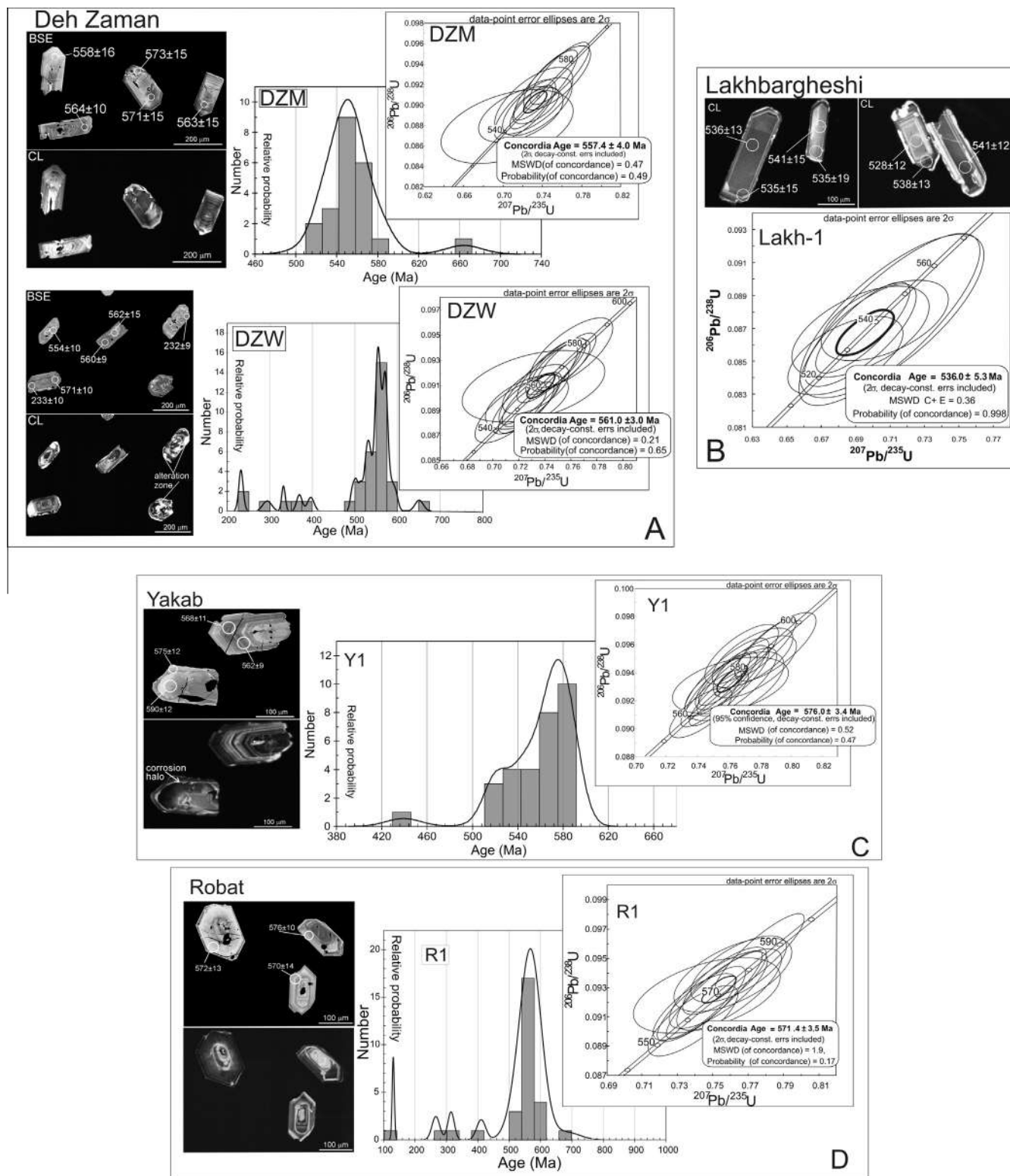


Fig. 11. U-Pb zircon systematics for the studied samples. (A) Deh Zaman pluton (samples DZM, DZW). (B) Lakhbargheshi pluton (sample Lakh-1). (C) Yakhab pluton (Y1 sample). (D) Robat (sample R1). BSE and cathodoluminescence images of selected zircon grains from the studied samples are shown, together with location of the LA-ICPMS laser spots (white circles). Concordia diagrams together with probability density plots showing the cumulative zircon data are also indicated. All ages are $^{206}\text{Pb}/^{238}\text{U}$ ages in Ma, with errors quoted at 2σ level.

few inherited cores. Seldom, fractured grains with metamictic textures are also observed that reveal unzoned and convoluted images. The Th/U ratios range 0.35–1.63 and the $^{206}\text{Pb}/^{238}\text{U}$ ages span from 439 to 590 Ma ($n = 30$). A total of fifteen concordant

analyses define a Concordia age of 576 ± 4 Ma (2σ , MSWD = 0.52) (Fig. 11C).

Robat The zircon separates from sample R1 show both prismatic to rounded/ovoid morphologies. The grains usually show

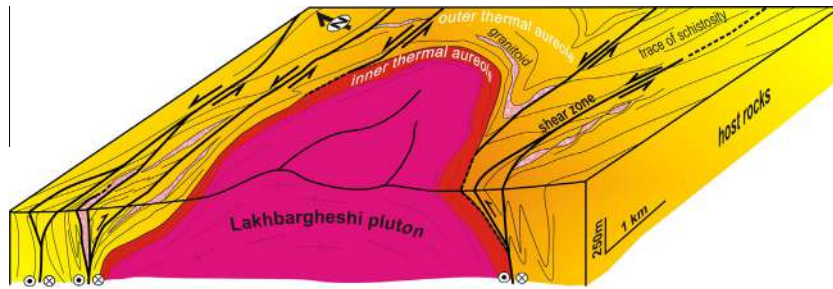


Fig. 12. Schematic 3-D block diagram to illustrate the syn-emplacement tectonic scenario for the Lakhbargheshi pluton under the control operated by regional sinistral transpressional shearing during early Cambrian times. In the host rocks, the shear zones vanish when entering the inner thermal aureole, as attested by a progressive transition from amphibolite-grade plano-linear shear fabrics to static, well annealed, textures.

oscillatory and sector growth zoning, with only limited evidence of secondary alteration. The Th/U ratios span 0.39–1.35, with the $^{206}\text{Pb}/^{238}\text{U}$ ages spanning from 130 to 685 Ma ($n = 30$). A population of eleven concordant analyses define a Concordia age of 571 ± 3 Ma (2σ , MSWD (concordance) = 1.9) (Fig. 11D).

7. Discussion

7.1. Structural interpretation

Field and structural data from the Kuh e Sarhangi region have documented the occurrence of distributed, NE–SW striking high angle mylonitic shearing that affect both the country rocks (Proterozoic Cambrian basement sequences) and the exposed granitoid intrusives with high angle dip values. Partitioning between regional strike slip and contractional deformation is widespread in the study area. The upright isoclinal folds overprinting regional foliation are always related to the proximity of a strike slip shear zone and suggest a close relationship between shortening and wrenching. Collectively, the structural framework and deformation fabrics that characterise the ductile shear belts described in this study point to a major transpressional regime, with simultaneous flattening (pure shear) and simple shear (oblique to dip slip shearing) on sub vertical planes (cf. Sanderson and Marchini, 1984; Tikoff and Fossen, 1993).

In order to reconstruct the sequential development of the ductile shearing in the study area, particularly relevant are the reconstructed field and textural relationships between shear fabrics development and granitoid texture/deformation. These relationships document overprinting and cross cutting relationships between the sequential development of the tectonic, magmatic, and metamorphic features in the study area. The majority of the exposed plutons (Deh Zaman, Yakhb and Robat) have been deformed during ductile regional transpression. In particular, the quartz feldspar microfabrics (microtextures consisting of myrmekite, mechanical twinning and, locally, recrystallised grains; augens of feldspar are present as well) document thermobaric conditions compatible with greenschist to amphibolite grade metamorphic conditions (e.g. Passchier and Trouw, 2005). On the other hand, the Lakhbargheshi pluton shows only limited evidence of tectonic deformation and primary magmatic fabrics are well preserved. In the host rocks, the amphibolite grade plano linear mylonitic shear fabrics vanishes when approaching the Lakhbargheshi intrusion, where it is progressively replaced by a well annealed amphibolite static fabric, concordant with the pluton host rock contact. This field evidence suggests high grade fabric development in the host rocks consistent with the regional ductile transpressional shear strain, in a continuum of magmatic through solid state deformation. The Lakhbargheshi pluton is thus considered as a syn tectonic intrusive body, emplaced during the general

SW–NE sinistral transpressional regime (Fig. 12). Consequently, despite direct dating of the syn kinematic shear zone assemblages are not yet available, the time lapse of transpressional shearing nucleation and development can be reasonably bracketed between the crystallisation ages of the ductile sheared intrusions (Deh Zaman Yakhb and Robat plutons) and that of the syn tectonic Lakhbargheshi intrusion.

7.2. Age of magmatism

The internal morphology and structures of the analysed zircon grains and the elevated Th/U ratios are typical of zircons of igneous origin (e.g. Belousova et al., 2002; Harley et al., 2007). Therefore, the obtained U–Pb Concordia ages can be assumed as the crystallisation ages of the Kuh Sarhangi intrusives. Our results document Late Neoproterozoic–Early Cambrian (Edacarian) ages, spanning between ca. 575 and 535 Ma. In particular, the older ages are derived from the ductile sheared intrusives (from SW to NE: Yakhb, Robat and Deh Zaman granites), while the younger Concordia age is obtained for the syn tectonic Lakhbargheshi pluton. The intimate linkage between deformation, metamorphism and pluton emplacement documented in this study supports and refines the previously published zircon U–Pb ages reported for the basement rocks of the tectonic zone (Ramezani and Tucker, 2003) and are in agreement with those reported from the Chahjam Biarjmand region (Shafaii Moghadam et al., in press) and from NW Iran (Azizi et al., 2011; Hassanzadeh et al., 2008; Jamshidi Badr et al., 2013; Fig. 1b) providing conclusive evidence for a dominant Cadomian signature of the metamorphic basement of Iran. No evidence is instead provided for the Tertiary high grade and magmatic events documented south eastward in the Saghand region (Verdel et al., 2007; Karagaranbafghi et al., 2012), attesting for differential exhumation/tectonic histories can be expected along the Kashmar Kerman Tectonic Zone during the Tertiary time lapse.

7.3. Petrogenesis and tectonic setting of the Kuh e Sarhangi magmatism

The granitic rocks of the Kuh e Sarhangi region have trace and REE characteristics similar to arc related granites and show comparable compositions with those reported from the Cadomian (Ediacaran–Cambrian) intrusives in Iran (Ramezani and Tucker, 2003; Hassanzadeh et al., 2008; Jamshidi Badr et al., 2013; Shafaii Moghadam et al., in press; Figs. 7 and 8). Significantly, based on the high SiO_2 contents, their REE and trace element patterns (Fig. 8A and B), and some of the trace element contents and ratios (e.g., $\text{Th} = 13.3\text{--}23.5$ ppm, $\text{U} = 1.6\text{--}3.2$ ppm, and $\text{Eu}^* < 1$), a significant crustal component (cf. Rudnick and Fountain, 1995; Patiño Douce and Beard, 1995) was likely involved in the generation of these granitic melts. These are general geochemical characteristics

of the early Cambrian magmatic rocks from Central Iran, which are dominated by acidic intrusives with prominent negative Eu anomaly (Ramezani and Tucker, 2003; Shafaii Moghadam et al., in press). The Central Iran is suggested to have a Mesoproterozoic crystalline basement, based on Sr Nd isotope systematics and zircon Hf isotope results from the Cadomian granitic rocks of the ChahJam Biarjmand area (Shafaii Moghadam et al., in press). The zircon U Pb Hf isotopic results reported in Nutman et al. (2014) confirms this hypothesis, indicating generation of the Cadomian magmatism from a mixture of juvenile Neoproterozoic and Archean sources. The Cadomian magmatism of the Iranian region can be thus tentatively interpreted as partial melting products of this crustal basement with minor mafic magma contribution. Similar magmatic scenarios dominated by crustal anatexis have been also proposed for the Early Paleozoic production of voluminous siliceous magmas all along the proto Tethyan active margin of Gondwana (Cawood et al., 2007; Zhu et al., 2012; Hu et al., 2013 and references therein).

The presence of magmatic epidote (Ps_{20-26}) in the Kuh e Sarhangi granites, with a composition comparable to those observed in North America Cordillera granitoids (Zen and Hammastrom, 1984; Zen, 1985; Dawes and Evans, 1991), suggests a melt origin and crystallisation/emplacement at moderately to high pressure (≥ 6.8 kbar; e.g. Zen and Hammastrom, 1984; Schmidt and Thompson, 1996; Schmidt and Poli, 2004; Chang and Andronicos, 2009). This is in agreement with (i) occurrence of Grs rich and Sps poor garnet in the magmatic assemblage, since the Grs end member increases in garnet with increasing pressure (>6 kbar), whereas a higher Sps content ($\text{MnO} > 4$ wt%) stabilises garnet at shallow depths (cfr. Harangi et al., 2001 and reference therein); (ii) results as derived from multiequilibrium and forward modelling thermobarometry, which document a $P-T$ range of magma emplacement for the Lakhbarghesi pluton compatible with the upper pressure field of the amphibolite facies; and (iii) the REE pattern reported in this study, which documents flat and relatively high HREE contents (Fig. 8A), suggesting HREE concentration in the residual melt during progress of partial melting at relatively high pressure (garnet stability depths). In particular, assuming an average rock density of 2600 kg m^{-3} , results from thermobarometric calculations indicate a depth of emplacement of ca. 40 km, which suggests magma intrusion in a thickened continental crust setting (Fig. 10).

Similarly to what proposed by Shafaii Moghadam et al. (in press) for the ChahJam Biarjmand region, we can thus assert that the Kashmar Kerman tectonic zone (Ramezani and Tucker, 2003), where the Kuh e Sarhangi region is located, exposes the exhumed roots of a Cadomian (Ediacaran Cambrian) magmatic arc, where early Cambrian sinistral transpression accommodated tectonic convergence and emplacement of the dominantly anatectic melts generated at the base of the thickened Pre Cambrian continental crust by subduction related (ultra)mafic magma underplating. The Early Cambrian (ca. 535 Ma) transpressional shear development and magmatism documented in this study is thus interpreted as the upper plate response to oblique subduction of the proto Tethyan ocean along the northern margin of the Gondwana Supercontinent.

8. Implication for the Gondwana assembly

The results of the present study support previous reconstructions, which place Central Iran in an active convergent setting scenario in the course of Ediacaran Cambrian times, during formation of an Andean type margin all along the proto Tethyan convergent margin of northern Gondwana (e.g., Cawood et al., 2007; Saki, 2010; Hu et al., 2013; Shafaii Moghadam et al., in press and references therein). This major geodynamic event occurred between ca.

580 and 500 Ma, when initiation of oceanic slab subduction along the peri Gondwana margins and collision between the various continental components inboard caused the final assembly of the Gondwana Supercontinent (Meert, 2003; Collins and Pisarevsky, 2005; Cawood and Buchan, 2007; Murphy et al., 2011; Zhu et al., 2012).

The results also provide new constraints on the time frame and tectonic processes involved in magma segregation and emplacement during the Gondwana assembly in Iran. Significantly, our zircon U Pb data set dates back the Cadomian arc formation in the Cimmerian Terranes of Iran to late Proterozoic times and document a ca. 40 Ma history of magmatic arc construction, spanning from ca 575 to 535 Ma. This evidence implies a stable, long lived arc or arcs in which intermittent magmatism occurred concurrently with oceanic subduction all along the proto Tethyan margin since late Proterozoic times and continued through the early Paleozoic.

Magma emplacement related to transpressional zones suggests for an oblique convergent setting, where calcalkaline magmas were collected from deep crustal sources and channelled to higher crustal levels along steeply dipping crustal discontinuities during crustal shortening and thickening (e.g., Saint Blanquat et al., 1998). An oblique convergence scenario is thus proposed for the Early Paleozoic consumption of the proto Tethyan oceanic lithosphere and the setting for subduction related Cadomian arc construction along the northern margin of the Gondwana Supercontinent.

Acknowledgements

We acknowledge logistic support in the field provided by the Tarbiat Modares University. We thank M. Mohajjel and A. Yassaghi for discussion and advice in the field. We are grateful to A. Zanchi, H. Shafaii Moghadam and an anonymous reviewer for constructive advice and comments that contributed to improve the manuscript. Projection and analysis of the structural data was performed through the software DAISY3 (<http://host.uniroma3.it/progetti/fra/lab/Downloads/Programs/>). Financial support provided by the Darius Programme.

Appendix A. – Analytical methods

A.1. Mineral chemistry

Mineral compositional data were obtained using a Camebax SX100 electron microprobe at the Institut für Mineralogie, Universität Stuttgart. Operating conditions were 15 kV and a 15 nA beam current (WDS mode). Mineral compositions were determined rela-

tive to natural and synthetic standards. Spot sizes were $1-10 \mu\text{m}$ depending on the phases analysed. Concentration maps for major elements (Ca, Fe, Mn, Mg and Al or Na) were also produced by step-wise movements of the thin sections under the electron beam; counting times per step were 100 ms. BSE imaging was obtained by using the same electron microprobe. Operating conditions were: 15 kV and 20 nA. Classification of amphibole with the general formula $\text{AB}_2\text{C}_5\text{T}_8\text{O}_{22}(\text{OH})_2$ has been made according to the IMA recommendations (Leake et al., 2004), by means of the WINAMPHCAL software of Yavuz (2007). Other mineral structural formulae were calculated through the software Ax enclosed in the THERMOCALC package.

A.2. Whole rock geochemistry

Samples selected for geochemistry were grounded in a pre-contaminated agate mill after careful washing in distilled water. The chemical analyses of the Kuh e Sarhangi samples were

performed at the Activation Laboratory (Ontario, Canada), through ICP emission (major and some trace elements) and ICP MS for trace elements (Code of analyses WRA + TRACE 4 Lithoresearch). For major elements the precision is estimated better than 2% for values higher than 5 wt% and better than 5% in the range 0.1–5 wt%. For trace elements and REE the precision is 5% in the range 1–100 ppm and 10% in the range 0.1–1 ppm.

A.3. U–Th–Pb isotope analyses

Uranium, thorium and lead isotopes were analyzed using a ThermoScientific Element 2 sector field ICP MS coupled to a Resolution M 50 (Resonetics) 193 nm ArF excimer laser (CompexPro 110, Coherent) system at Goethe University Frankfurt (GUF). Data were acquired in time resolved peak jumping pulse counting/analogue mode over 480 mass scans, with a 20 s background measurement followed by 21 s sample ablation following the method described in Gerdes and Zeh (2006, 2009) and Frei and Gerdes (2009). All data was corrected using GJ 1 zircon as primary standard. The total offset of the measured drift corrected $^{206}\text{Pb}/^{238}\text{U}$ ratio ($n = 14$; 2 SD $\sim 1.3\%$) from the “true” ID TIMS value (0.0982 ± 0.0004 ; ID TIMS GUF value) of the analyzed GJ 1 grain was around 6% and the drift over the day was less than 1%. The accuracy of the method was verified by analyses of reference zircon 91500 (1062 ± 6.9 Ma, MSWD of concordance and equivalence = 0.98, $n = 10$), and Plešovice (337.8 ± 4.2 Ma, MSWD_{C+E} = 0.58, $n = 8$) during that analytical session.

Appendix B. Appendix – Petrographic description of the dated samples

B.1. Deh Zaman (samples DZW and DZM)

The Deh Zaman samples are characterised by inequigranular olocrystalline texture with a primary igneous mineralogy made of Qtz, Pl (An_{6-21}), Kfs (Ab_{2-7}), Ab (Or_{0-2}) + Grt ($\text{Alm}_{57-67}\text{GrS}_{18-24}\text{Py}_{5-9}\text{Sps}_{4-12}$) + Bt (TiO_2 up to 3.90 wt%) + Zrn + Ap. Post magmatic mineral growth is attested by chloritisation of biotite and secondary crystallisation of white mica epidote aggregates replacing pristine igneous plagioclase.

B.2. Lakhbargheshi (sample Lakh 1)

Leucocratic body with micro granular to coarse grained texture. Primary igneous assemblage consists of Qz, Kfs (Ab_{1-11}), Ab (Or_{0-2}) + Ep (Ps_{20-26}) + Grt ($\text{Alm}_{36-42}\text{GrS}_{42-46}\text{Py}_{13-18}\text{Sps}_{13-18}$) + Bt ($\text{TiO}_2 = 1.24\text{--}3.01$ wt%) + Zrn + Ttn + Ap. Alteration of biotite to form chlorite, together with late crystallisation of secondary epidote (Ps_{17-20}) and white micas aggregates replacing alkali feldspars are usually observed.

B.3. Yakhhab (sample Y1) and Robat (sample R1)

Granite texture is inequigranular faneritic olocrystalline, with primary igneous mineralogy made of Qz, Pl (An_{14-31}), Kfs (Ab_{1-22}), Ab (Or_{5-21}) + Ep (Ps_{21}) + Grt ($\text{Alm}_{62-70}\text{GrS}_{23-31}\text{Py}_{2-9}\text{Sps}_{0-3}$) + Bt ($\text{TiO}_2 = 1.31\text{--}2.42$ wt%) + Ilm + Zrn + Ap. Late crystallisation of secondary epidote as micro aggregates on plagioclase, secondary growth of white micas replacing alkali feldspars, together with biotite chloritisation are commonly observed.

References

Alavi, M., 1991. Sedimentary and structural characteristics of the Paleo-Tethys remnants in northeastern Iran. *Geol. Soc. Am. Bull.* 103, 983–992.

- Azizi, H., Chung, S.L., Tanaka, T., Asahara, Y., 2011. Isotopic dating of the Khoy metamorphic complex (KMC), northwestern Iran: a significant revision of the formation age and magma source. *Precamb. Res.* 185, 87–94.
- Bagheri, S., Stampfli, G.M., 2008. The Anarak, Jandaq and Posht-e-Badam metamorphic complex in central Iran: new geological data, relationships and tectonic implications. *Tectonophysics* 451, 123–155.
- Belousova, E.A., Griffin, W.L., O'Reilly, S.Y., Fisher, N.I., 2002. Igneous zircons: trace element composition as an indicator of source rock type. *Contrib. Miner. Petrol.* 143, 602–622.
- Berberian, M., 1981. Active faulting and tectonics of Iran. In: Gupta, H.K., Delany, F.M. (Eds.), *Zagros-Hindu Kush-Himalaya Geodynamic Evolution*, vol. 3, American Geophysical Union Geodynamic Series, pp. 33–69.
- Berberian, M., King, G.C.P., 1981. Towards a paleogeography and tectonic evolution of Iran. *Can. J. Earth Sci.* 18, 210–265.
- Berra, F., Angiolini, L., 2014. The evolution of the Tethys region throughout the Phanerozoic: a brief tectonic reconstruction. In: Marlow, L., Kendall, C., Yose, L. (Eds.), *Petroleum Systems of the Tethyan Region*, vol. 106. The American Association of Petroleum Geologists, pp. 1–27, doi:10.1306/13431840M1063606.
- Boger, S.D., Miller, J.M., 2004. Terminal suturing of Gondwana and the onset of the Ross-Delamerian Orogeny: the cause and effect of an Early Cambrian reconfiguration of plate motions. *Earth Planet. Sci. Lett.* 219, 35–48.
- Bucher, K., Frey, M., 2002. *Petrogenesis of Metamorphic Rocks*, seventh ed. Springer-Verlag, Berlin.
- Cawood, P.A., 2005. Terra Australis Orogen: Rodinia breakup and development of the Pacific and Iapetus margins of Gondwana during the Neoproterozoic and Paleozoic. *Earth-Sci. Rev.* 69, 249–279.
- Cawood, P.A., Buchan, C., 2007. Linking accretionary orogenesis with supercontinent assembly. *Earth Sci. Rev.* 82, 217–256.
- Cawood, P.A., Johnson, M.R.W., Nemchin, A.A., 2007. Early palaeozoic orogenesis along the Indian margin of Gondwana: Tectonic response to Gondwana assembly. *Earth Planet. Sci. Lett.* 255, 70–84.
- Collins, A.S., Pisarevsky, S.A., 2005. Amalgamating eastern Gondwana: the evolution of the Circum-Indian Orogens. *Earth-Sci. Rev.* 71, 229–270.
- Connolly, J.A.D., 2005. Computation of phase equilibria by linear programming: a tool for geodynamic modeling and its application to subduction zone decarbonation. *Earth Planet. Sci. Lett.* 236, 524–541.
- Chang, J.M., Andronikos, C.M., 2009. Constraints on the depth of generation and emplacement of a magmatic epidote-bearing quartz diorite pluton in the Coast Plutonic Complex, British Columbia. *Terra Nova* 21, 480–488.
- Dalziel, I.W.D., 1991. Pacific margins of Laurentia and East Antarctica-Australia as a conjugate rift pair: evidence and implications for an Eocambrian supercontinent. *Geology* 19, 598–601.
- Dawes, R.L., Evans, B.W., 1991. Mineralogy and geothermobarometry of magmatic epidote-bearing dikes, Front Range, Colorado. *Geol. Soc. Am. Bull.* 103, 1017–1031.
- Defant, M.J., Drummond, M.S., 1990. Derivation of some modern arc magmas by melting of young subducted lithosphere. *Nature* 347, 662–665, 10.1038/347662a0.
- Eftekharneshad, Nabavi J., Ruttner M.H., Valeh A., Alavi N., Hajian M., Haghighpour J.A., 1977. Geological map of Ferdows (1:250000). Geological survey of Iran.
- Frei, D., Gerdes, A., 2009. Accurate and precise in-situ zircon U–Pb age dating with high spatial resolution and high sample throughput by automated LA-SF-ICP-MS. *Chem. Geol.* 261, 261–270.
- Gerdes, A., Zeh, A., 2006. Combined U–Pb and Hf isotope LA-(MC)-ICP-MS analyses of detrital zircons: comparison with SHRIMP and new constraints for the provenance and age of an Armorican metasediment in Central Germany. *Earth Planet. Sci. Lett.* 249, 47–62.
- Gerdes, A., Zeh, A., 2009. Zircon formation versus zircon alteration—new insights from combined U–Pb and Lu–Hf in situ LA-ICP-MS analyses, and consequences for the interpretation of Archean zircon from the Central Zone of the Limpopo Belt. *Chem. Geol.* 261, 230–243.
- Gessner, K., Collins, A.S., Ring, U., Gungör, T., 2004. Structural and thermal history of poly-orogenic basement: U–Pb geochronology of granitoid rocks in the southern Menderes Massif, Western Turkey. *J. Geol. Soc., London* 161, 93–101.
- Harangi, S.Z., Downes, H., Kósa, L., Szabó, C.S., Thirlwall, M.F., Mason, P.R.D., Matthey, D., 2001. Almandine garnet in calc-alkaline volcanic rocks of the Northern Pannonian Basin (Eastern-Central Europe): geochemistry, petrogenesis and geodynamic implications. *J. Petrol.* 42, 1813–1843.
- Harley, S.L., Kelly, N.M., Möller, A., 2007. Zircon behaviour and the thermal histories of mountain chains. *Elements* 3, 25–30.
- Hassanzadeh, J., Stockli, D.F., Horton, B.K., Axen, G.J., Stockli, L.D., Grove, M., Schmitt, A.K., Walker, J.D., 2008. U–Pb zircon geochronology of late Neoproterozoic–Early Cambrian granitoids in Iran: implications for paleogeography, magmatism, and exhumation history of Iranian basement. *Tectonophysics* 451, 71–96.
- Horton, B.K., Hassanzadeh, J., Stockli, D.F., Axen, G.J., Gillis, R.J., Guest, B., Amini, A., Fakhari, M.D., Zamanzadeh, S.M., Grove, M., 2008. Detrital zircon provenance of Neoproterozoic to Cenozoic deposits in Iran: implications for chronostratigraphy and collisional tectonics. *Tectonophysics* 451, 97–122.
- Hu, P., Li, C., Wang, M., Xie, C., Wu, Y., 2013. Cambrian volcanism in the Lhasa terrane, southern Tibet: record of an early Paleozoic Andean-type magmatic arc along the Gondwana proto-Tethyan margin. *J. Asian Earth Sci.* 77, 91–107.
- Jafari, S.M., Shemirani, A., Hamdi, B., 2007. Microstratigraphy of the Late Ediacaran to Ordovician in NW Iran (Takab area). In: Vickers-Rich, P., Komarow, P. (Eds.), *The Rise and Fall of the Ediacaran Biota*, vol. 286, Geological Society, London, Special Publications, pp. 433–437.

- Jamshidi Badr, M., Collins, A.S., Masoudi, F., Cox, G., Mohajjel, M., 2013. The U-Pb age, geochemistry and tectonic significance of granitoids in the Soursat Complex, Northwest Iran. *Turkish J. Earth Sci.* 22, 1–31.
- Karagaranbafghi, F., Foeken, J.P.T., Guest, B., Stuart, F.M., 2012. Cooling history of the Chapedony metamorphic core complex, Central Iran: implications for the Eurasia-Arabia collision. *Tectonophysics* 524–525, 100–107.
- Leake, B.E., Alan, R.W., William, D.B., Ernst, A.J.B., Giovanni, F., Jeol, D.J., Frank, C.H., Hanan, J.K., Vladimir, G.K., John, C.S., Nicholas, C.N.S., Eric, J.W.W., 2004. Nomenclature of amphiboles: additions and revisions to the International Mineralogical Associations amphibole nomenclature. *Am. Mineral.* 89, 883–887.
- Le Maitre, R.W., 2002. *Igneous Rocks: A Classification and Glossary of Terms*, second ed. Cambridge University Press, Cambridge, UK, p. 236.
- Li, Z.X., Bogdanova, S.V., Collins, A.S., Davidson, A., DeWaele, B., Ernst, R.E., Fitzsimons, I.C.W., Fuck, R.A., Gladkochub, D.P., Jacobs, J., Karlstrom, K.E., Lu, S., Natapov, L.M., Pease, V., Pisarevsky, S.A., Thrane, K., Vernikovsky, V., 2008. Assembly, configuration, and break-up history of Rodinia: a synthesis. *Precamb. Res.* 160, 179–210.
- Ludwig, K., 2003. User's manual for Isoplot/Ex v3.0, a geochronological toolkit for Microsoft Excel, vol. 4. Berkeley Geochronology Center, Special Publication, pp. 25–31.
- Martin, H., 1999. Adakitic magmas: modern analogues of Archean granitoids. *Lithos* 46, 411–429.
- Mahmoud, R.I., Faryad, S.W., Holub, F.V., Košler, J., Frank, W., 2011. Magmatic and metamorphic evolution of the Shotur Kuh metamorphic complex (Central Iran). *Int. J. Earth Sci.* 100, 45–62.
- Meert, J.G., 2003. A synopsis of events related to the assembly of eastern Gondwana. *Tectonophysics* 362, 1–40.
- Meert, J.G., Lieberman, B.S., 2008. The Neoproterozoic assembly of Gondwana and its relationship to the Ediacaran-Cambrian radiation. *Gondwana Res.* 14, 5–21.
- Murphy, J.B., van Staal, C.R., Collins, W.J., 2011. A comparison of the evolution of arc complexes in Paleozoic interior and peripheral orogens: speculations on geodynamic correlations. *Gondwana Res.* 19, 812–827.
- Nozaem, R., Mohajjel, M., Rossetti, F., Della Seta, M., Vignaroli, G., Yassaghi, A., Salvini, S., Eliassi, M., 2013. Post-Neogene right-lateral strike-slip tectonics at the north-western edge of the Lut Block (Kuh-e-Sarhangi Fault), Central Iran. *Tectonophysics* 589, 220–233.
- Nance, R.D., Murphy, J.D., Santosh, M., 2014. The supercontinent cycle: a retrospective essay. *Gondwana Res.* 25, 4–29.
- Nutman, A.P., Mohajjel, M., Bennet, V.C., Fergusson, C.L., 2014. Gondwanan Eoarchean-Neoproterozoic ancient crustal material in Iran and Turkey: zircon U–Pb–Hf isotopic evidence. *Can. J. Earth Sci.* 51, 272–285.
- Passchier, C.W., Trouw, R.A.J., 2005. *Microtectonics*, second ed. Springer Verlag, Berlin-New York, 366pp.
- Patiño Douce, A.E., Beard, J.S., 1995. Dehydration-melting of biotite gneiss and quartz amphibolite from 3 to 15 kbar. *J. Petrol.* 36, 707–738.
- Pearce, J.A., Harris, N.B.W., Tindle, A.G., 1984. Trace element discrimination diagrams for the tectonic interpretation of granitic rocks. *J. Petrol.* 25, 956–983, 10.1093/petrology/25.4.956.
- Peccerillo, A., Taylor, S.R., 1976. Geochemistry of Eocene calc-alkaline volcanic rocks from the Kastamonu area, northern Turkey. *Contrib. Mineral. Petr.* 58, 63–81. <http://dx.doi.org/10.1007/BF00384745>.
- Powell, R., Holland, T.J.B., 1994. Optimal geothermometry and geobarometry. *Am. Mineral.* 79, 120–133.
- Powell, R., Holland, T.J.B., 2008. On thermobarometry. *J. Metamorph. Geol.* 26, 155–179.
- Ramezani, J., Tucker, R.D., 2003. The Saghand region, central Iran: U–Pb geochronology, petrogenesis and implications for Gondwana tectonics. *Am. J. Sci.* 303, 622–665.
- Rudnick, R.L., Fountain, D.M., 1995. Nature and composition of the continental crust: a lower crustal perspective. *Rev. Geophys.* 33, 267–309.
- Rutner, A., Nabavi, M.H., Alavi, M., 1970. Geological map of Ozbak Kuh mountain (1/100,000). Geological survey of Iran.
- Sanderson, D., Marchini, R.D., 1984. Transpression. *J. Struct. Geol.* 6, 449–454.
- Sahandi, M., Baumgartner, S., Schmidt, K., 1983. Contributions to the stratigraphy and tectonics of the Zeber-Kuh Range (East Iran). *Neues Jahrbuch für Geologie und Paläontologie, Abhandlungen* 168, 346–357.
- Sahandi, M., Ghassemi, M.R., Ekhtiarabadi, Y., 2011. Geological map of Ghasemabad (1:100,000). Geological Survey of Iran.
- Saint Blanquat, M., Tikoff, B., Teyssier, C., Vigneresse, J.L., 1998. Transpressional kinematics and magmatic arcs. In: Holdsworth, R.E., Strachan, R.A., Dewey, J.F. (Eds.), *Continental Transpression and Transtension Tectonics*, vol. 135. Geological Society of London Special Publication, pp. 327–340.
- Saki, A., 2010. Proto-Tethyan remnants in northwest Iran: geochemistry of the gneisses and metapelitic rocks. *Gondwana Res.* 17, 704–714.
- Schmidt, M.W., Poli, S., 2004. Magmatic epidote. *Rev. Mineral. Geochem.* 56, 399–430.
- Schmidt, M.W., Thompson, A.B., 1996. Epidote in calc-alkaline magmas: an experimental study of stability, phase relationships, and the role of epidote in magmatic evolution. *Am. Mineral.* 81, 462–474.
- Sengör, A.M.C., 1984. The Cimmeride orogenic system and the tectonics of Eurasia. *Geological Society of America Special Paper*, 195pp.
- Shafaii Moghadam, H.S., Khademi, M., Hu, Z., Stern, R.J., Santos, J.F., Wue, Y., 2013. Cadomian (Ediacaran–Cambrian) arc magmatism in the Chahjam–Biarjmand metamorphic complex (Iran): Magmatism along the northern active margin of Gondwana. *Gondwana Res.* <http://dx.doi.org/10.1016/j.gr.2013.10.014>, in press.
- Spear, F.S., 1993. *Metamorphic Phase Equilibria and Pressure–Temperature–Time paths*. Monograph Mineralogical Society of America, Washington, DC.
- Stacey, J.S., Kramers, J.D., 1975. Approximation of terrestrial lead isotope evolution by a 2-stage model. *Earth Planet. Sci. Lett.* 26, 207–221.
- Stocklin, J., Ruttner, A., Nabavi, M., 1964. New data on the Lower Paleozoic and pre-Cambrian of North Iran. *Geological Survey of Iran, Report* 1, 29p.
- Stöcklin, J., 1968. Structural history and tectonics of Iran: a review. *Am. Assoc. Pet. Geol. Bull.* 52, 1229–1258.
- Streckeisen, A.L., Le Maitre, R.W., 1979. A chemical approximation to the modal QAPF classification of the igneous rocks. *Neues Jahrbuch für Mineralogie, Abhandlungen* 136, 169–206.
- Sun, S.S., McDonough, W.F., 1989. Chemical and isotopic systematics of oceanic basalts: Implications for mantle composition and processes. In: Saunders, A.D., Norry, M.J. (Eds.), *Magmatism in Ocean Basins*, vol. 42. Geological Society of London Special Publication, pp. 312–345.
- Takin, M., 1972. Iranian geology and continental drift in the Middle East. *Nature* 235, 147–150.
- Tikoff, B., Fossen, H., 1993. Simultaneous pure and simple shear: the unified deformation matrix. *Tectonophysics* 217, 115–117.
- Torsvik, T.H., Cocks, L.R.M., 2013. Gondwana from top to base in space and time. *Gondwana Res.* 24, 999–1030.
- Torsvik, T.H., Cocks, L.R.M., 2009. New Zealand northeastern and eastern peri-Gondwanan margin from Turkey to New Zealand. In: Bassett, M.G. (Ed.), *Early Palaeozoic Peri-Gondwana Terranes: New Insights from Tectonics and Biogeography*, vol. 325. Geological Society, London, Special Publications, pp. 3–21. doi: 10.1144/SP325.2 0305–8719/09.
- Ustaömer, P.A., Ustaömer, T., Collins, A.S., Robertson, A.H.F., 2009. Cadomian (Ediacaran–Cambrian) arc magmatism in the Bitlis Massif, SE Turkey: magmatism along the developing northern margin of Gondwana. *Tectonophysics* 473, 99–112.
- Verdel, C., Wernicke, B.P., Ramezani, J., Hassanzadeh, J., Renne, P.R., Spelle, T.L., 2007. Geology and thermochronology of Tertiary Cordilleran-style metamorphic core complexes in the Saghand region of central Iran. *Bull. Geol. Soc. Am.* 119, 961–977. <http://dx.doi.org/10.1130/B26102.1>.
- Yavuz, F., 2007. WinAmphcal: a Windows program for the IMA-04 amphibole classification. *Geochem. Geophys. Geosyst.* 8, Q01004. <http://dx.doi.org/10.1029/2006GC001391>.
- Watson, E.B., Harrison, T.M., 1983. Zircon saturation revisited: temperature and composition effects in a variety of crustal magma types. *Earth Planet. Sci. Lett.* 64, 295–304, 10.1016/0012-821X(83)90211-X.
- Whitney, D.L., Evans, B.W., 2010. Abbreviations for names of rock forming minerals. *Am. Mineral.* 95, 185–187.
- Zen, E.A., 1985. Implications of magmatic epidote-bearing plutons on crustal evolution in the accreted terranes of northwestern North America. *Geology* 13, 266–269.
- Zen, E.A., Hammarstrom, J.M., 1984. Magmatic epidote and its petrologic significance. *Geology* 12, 515–518.
- Zhu, D.C., Zhao, Z.D., Niu, Y.L., Dilek, Y., Wang, Q., Ji, W.H., Dong, G.C., Sui, Q.L., Liu, Y.S., Yuan, H.L., Mo, X.X., 2012. Cambrian bimodal volcanism in the Lhasa Terrane, southern Tibet: record of an early Paleozoic Andean-type magmatic arc in the Australian proto-Tethyan margin. *Chem. Geol.* 328, 290–308.